AD-A091 085 AIR FORCE INST OF TECH WRIGHT-PATTERSON AFB OH SCHOO--ETC F/G 10/1
EXPERIMENTAL STUDY OF THE THERMAL PERFORMANCE PARAMETERS OF A L--ETC(U)
SEP 80 C D WOODRUM
UNCLASSIFIED AFIT/GAE/AA/80S-3 NL

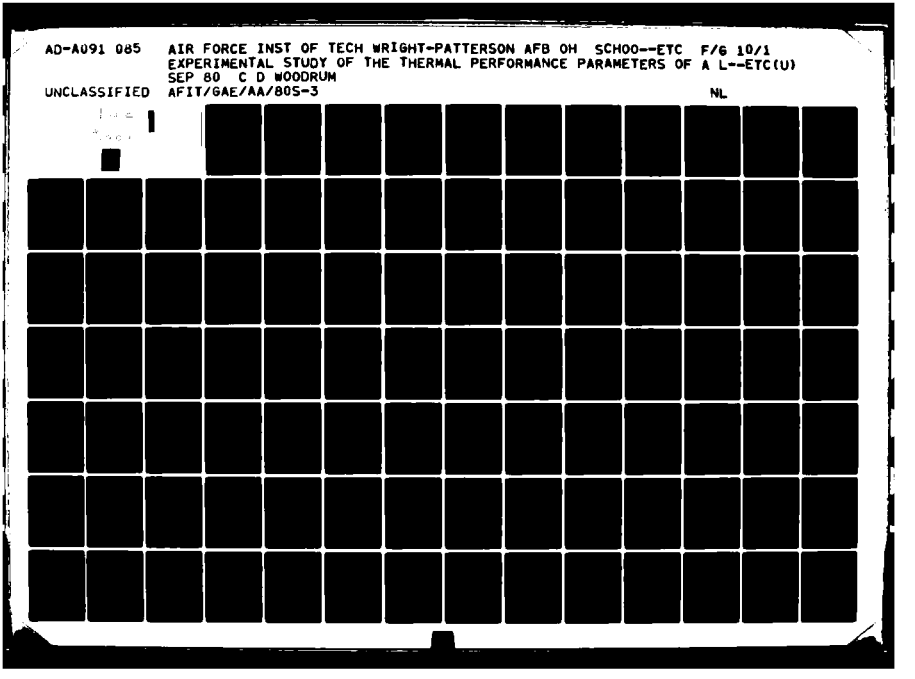

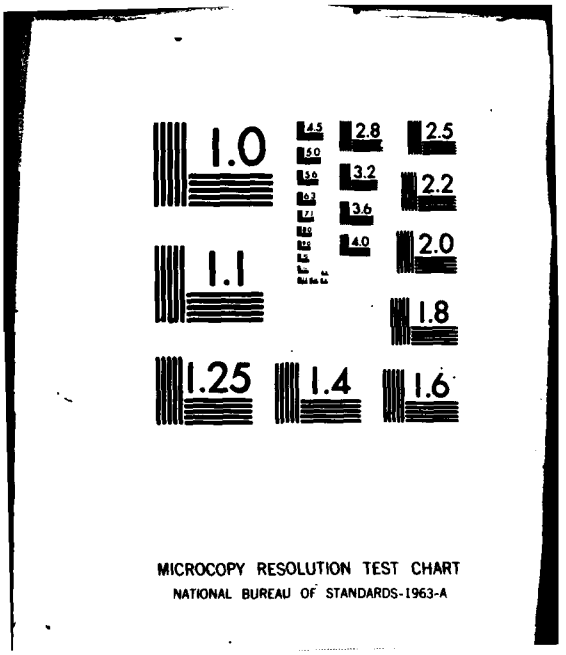
1.0
1.1
1.25
1.4
1.6
1.8
2.0
2.2
2.5
2.8
3.2
3.6
4.0
4.5
5.0
5.6
6.3
7.1
MICROCOPY RESOLUTION TEST CHART
NATIONAL BUREAU OF STANDARDS-1963-A

(14) AFIT/GAE/AA/80S-3

LEVEL II

(1)

(11) Sep 80

(12) 122

(6) EXPERIMENTAL STUDY OF THE THERMAL PERFORMANCE PARAMETERS OF A LIQUID-HEATING FLAT PLATE SOLAR COLLECTOR

(9) Master's THESIS

by

(10) Charles Dana Woodrum
AFIT/GAE/AA/80S-3

AFIT/GAE/AA/80S-3

EXPERIMENTAL STUDY OF THE THERMAL PERFORMANCE PARAMETERS OF A LIQUID-HEATING FLAT PLATE SOLAR COLLECTOR

THESIS

Presented to the Faculty of the School of Engineering

of the Air Force Institute of Technology

in Partial Fulfillment of the

Requirements for the Degree of

Master of Science

by

Charles Dana Woodrum

Graduate Aeronautical Engineering

September 1980

Preface

Solar energy is rapidly becoming a permanent fixture to the American way of life. Governmental research contracts, literature, businesses, and individual interests alike have literally skyrocketed since the 70's, and there is no end in sight. Likewise, my own interests in solar energy have progressed over the past few years due in part to the rising cost of energy. But more than this-I think-I really wonder if the marvelous mother earth who has so well provided for mankind since earliest history is not waning under the strain of our unquenchable and relentless quest for energy. What has taken her eons to produce, it has taken us only a few generations to use. How long can she sustain us or our progeny? She is patiently and silently awaiting relief.

Our energy consumption has been and will continue to be weighed. It is only a matter of time before the balance tips and decides our destiny. This feeling more than any other has left me with a challenge-a challenge to conserve energy, to explore new alternatives, and to find a better way to meet our energy needs. I hope to pass along this challenge to you as well.

I wish to thank Dr. James Hitchcock, my advisor, for his ideas, leadership, and patience. Graditude is also extended to Mr. William Baker and Mr. Harold Cannon for their technical support. A special thanks goes to my two children, Danille and Carrie, for putting up with so many fatherless days, and a special thanks to Vicki, my wife, who offered continual encouragement and labored tirelessly typing this manuscript.

Dana Woodrum

Contents

List of Figures

List of Tables

List of Notation

English Symbols	Quantity	Units
A_c	Collector area	ft^2
C_b	Bond Conductance	B/hr-ft-F
C_p	Specific heat of water	B/lbm-F
D	Tube outside diameter	ft
D_i	Tube inside diameter	ft
F	Fin efficiency	None
F'	Collector efficiency	None
F_R	Collector heat removal factor	None
Gr	Grashof number	None
Gr_m	Mean Grashof number	None
Gz	Graetz number	None
Gz_m	Graetz number based on mean properties	None
h_i	Internal heat transfer coefficient	$B/hr-ft^2-F$
h_o	External heat transfer coefficient	$B/hr-ft^2-F$
I	Solar insolation (Beam and Diffuse)	B/hr
k	Thermal conductivity	B/hr-ft-F
L	Fin Width	ft
Nu_m	Mean Nusselt number	None
Nu_x	Local Nusselt number	None
n	Number of tubes	None
Pr	Local Prandtl number	None
Pr_m	Mean Prandtl number	None
Q	Heat loss	B/hr
Q_u	Collector useful energy gain	B/hr

English Symbols		Units
Re_x	Local Reynolds number	None
R_i'	Thermal resistance between fin and fluid	hr-ft^2-F/B
t	Temperature	F
t_{fi}	Collector fluid inlet temperature	F
t_{fo}	Collector fluid exit temperature	F
t_{fm}	Mean fluid temperature	F
t_{pm}	Mean plate temperature	F
t_∞	Ambient temperature	F
U	Fin loss coefficient	B/hr-ft^2-F
U_L	Collector overall loss coefficient	B/hr-ft^2-F
U_t	Collector top loss coefficient	B/hr-ft^2-F
W	Flowrate	lbm/min or lbm/hr
Y	Tube length	ft
α	Absorptance	None
β	Coefficient of expansion	1/F
δ	Fin thickness	ft
ϵ_g	Glass emissivity	None
ϵ_p	Plate emissivity	None
λ	Radiation wavelength	μm
ρ	Density	lbm/ft^3
σ	Stefan-Boltzmann constant	B/hr-ft^2-R^4
τ	Transmittance	None
$(\overline{\tau\alpha})$	Effective transmittance absorptance product	None

Abstract

Five tests were conducted on a 4X4 foot liquid-heating flat plate solar collector for:

(1) Internal heat transfer coefficient-with and without turbulators
(2) Flow distribution
(3) Bond conductance-clamped and woven fins
(4) Long wavelength transmittance of Kalwall
(5) Overall loss coefficient-heat removal factor product.

Mean values of the internal heat transfer coefficients ranged between 98-114 B/hr-ft^2-F for tubes without turbulators. Values as high as 522 B/hr-ft^2-F were obtained with turbulators. The flow distribution was determined to be satisfactory if turbulators were left in the risers. Non-uniform flow occurred without them as evidenced by temperature differences as high as 30 F between the collector inlet and tube wall temperatures (measured midway between the headers). Bond conductance values ranged from 18.88 B/hr-ft-F to 1.57 B/hr-ft-F for the clamped and woven fins, respectively. The transmittance for .025 inch Kalwall at long wavelengths was determined to be on the order of five percent. The overall loss coefficient was not successfully measured, but based on a previously determined value of it, the heat removal factor as a function of flowrate was compared for all configurations.

EXPERIMENTAL STUDY OF THE THERMAL PERFORMANCE PARAMETERS OF A LIQUID-HEATING FLAT PLATE SOLAR COLLECTOR

I Introduction

Energy is a key ingredient to any industrialized society. Whether it be from petroleum, natural gas, wood, nuclear, or solar, energy commands ever increasing attention of the world's leading nations. As current sources become exhausted through use, waste, political crises, or the synergistic effects of population and industrial growth, the demand for energy will undoubtedly forge a new life style for people and nations.

It has already begun in the United States. Speed limit reductions to 55 mph, federally sponsored energy conservation programs, tax credits, gasoline lines, gas rationing plans, higher prices for commodities, and acute increases in energy costs are all ever present reminders that a change in life style and new challenges lie just around the corner. Thus, energy-a long standing premium to the small businessman and manufacturer alike-is rapidly becoming a premium to the individual consumer.

Solar energy-freely available and exhaustless-is a form of low grade thermal energy which can meet such needs as space heating, food drying, hot water supply and others for individuals and businesses. Furthermore it requires no hauling, refining, mining, drilling, or cleaning-and it is pollution free. The user simply traps it with the solar collector and transports it through a system of pipes or air ducts for immediate use or storage. The major stumbling block to this seemingly simple task is one of economics. Thus, solar energy designers are constantly striving

for efficient and maintenance free systems.

As energy is a key ingredient to a society efficiency is the key ingredient to any energy conversion system. Since solar collectors are the central components to any solar energy conversion system, the purpose of this study has been to investigate the thermal performance parameters which combine to define the efficiency and thermal worthiness of one. It has been limited to the liquid-heating flat plate type. Two plates-a clamped and woven fin-have been studied for bond conductance characteristics. The effects of an increased internal heat transfer coefficient have been studied. Flow distribution and long wavelength transmittance characteristics have also been examined. Lastly, the overall loss coefficient and the effect of flowrate on collector performance was investigated.

Previous work by Groves (Ref 5) examined the overall loss coefficient and collector efficiency by irradiating the collector with a solar simulator. In this study, however, the collector overall loss coefficient, internal heat transfer coefficient, bond conductance, and flow distribution were all evaluated by separate heat loss tests. The internal heat transfer coefficient test compared results with and without turbulators inserted. The flow distribution test gave an assessment of the validity of the uniform flow assumption instrumental to the development of the energy equation. The bond conductance test compared the effectiveness of the two types of absorber plates. The long wavelength transmittance test of the Kalwall covers showed how Kalwall performed in obstructing far infrared radiation. Lastly, the overall loss coefficient-heat removal factor product test attempted to determine the overall loss coefficient value and study the effect of flowrate on the collector's thermal performance.

II Flat Plate Collector Theory and Description

Solar collectors are the essential components to any solar energy conversion system. Although collectors are not unlike heat exchangers in that energy is transferred to a fluid, they have unique functions, problems and characteristics. The purpose of a solar collector is to absorb radiant energy from a distant source-the sun-and transfer that energy to a medium-air or water-for transport to a storage facility or for immediate use.

Many practical problems are encountered trying to implement this simple function. For instance, before the collector can operate, radiant energy has to be present. The incident energy outside the earth's thin layer of air is essentially constant beam radiation. But, after passage through the atmosphere, the beam radiation usually undergoes considerable absorption, reflection and scattering such that the useful radiation at the surface is significantly less than that originally available and is characterized by both beam and diffuse components. The problem of characterizing and predicting the available radiation has received considerable attention in the past, and, fortunately, predictions can now be made to a satisfactory degree.

The collector must be able to absorb both the beam and diffuse components of radiation and transfer it to the fluid with as small a loss as possible. This inherently means high fin efficiencies, bond conductances, and heat removal factors-terms to be defined later. It also means small loss coefficients and low absorber plate operating temperatures. A good design has a selective absorber plate (i.e. high absorption characteristics in the short wavelength range and low

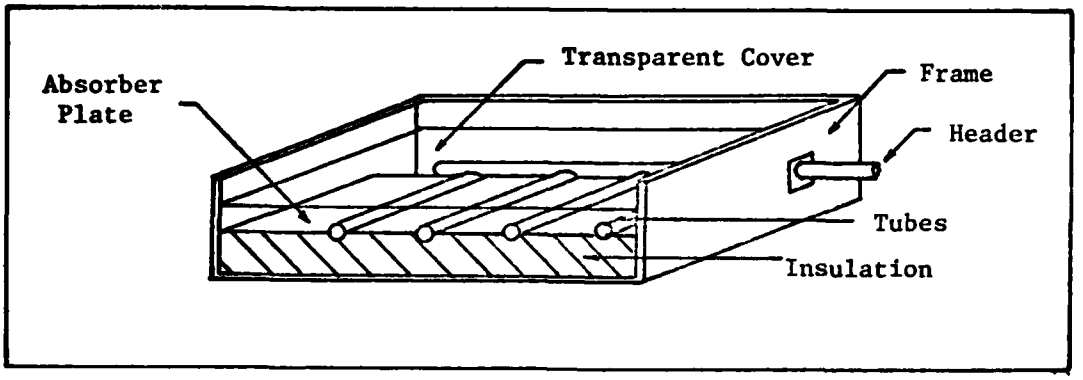

Figure 1 Basic Components of a Liquid Flat Plate Collector

emittance in the long wavelength range) as well as a cover system which transmits most of the solar energy and very little far infrared radiation. All these factors combine in the design of a solar collector to determine the overall thermal performance.

Solar collector designs are characterized by application, fluid transport medium, and geometry. Systems may be liquid heating or cooling, free or forced air systems, hybrid systems, or systems with concentrating collectors. One simple type is the liquid heating flat plate collector designed for residential hot water systems application.

General Description

The basic components of the liquid heating flat plate collector shown in Figure 1 are the absorber plate, covers, insulation, tubes, and frame. Each component has a special purpose. The transparent covers produce the so called greenhouse effect by permitting short wavelength solar radiation to pass through to the absorber plate but allowing very little long wavelength energy to be re-radiated. It also resists heat transfer losses by convection. The absorber plate collects the energy and conducts it

to the liquid filled tubes. It should have sufficient thickness and high conductivity so that fin efficiencies are 90 to 95 percent. Economic and installation considerations may preclude much higher values than these. The tubes and headers form the transport path of the fluid. The tubes must be firmly bonded to the absorber plate and have high internal heat transfer coefficients to maximize the heat transfer from the plate to the liquid. The pipe system must also be sized such that the pressure drop considerations result in uniform flow, otherwise, local hot spots on the collector develop and degrade performance. Lastly, the frame offers architectural style, rigidness, and also serves to reduce heat loss.

Figure 1 shows a parallel flow type collector, but others such as serpentine flow types are available. There are also many ways of forming the bond between the fins and tubes. Several ways are examined later.

The collector used in this investigation was a liquid-heating flat plate collector similiar to that shown in Figure 1. The absorber plate was a 4X4 foot, .035 inch thick steel sheet plated with copper to prevent corrosion. The absorber plate was made with smaller platelets each four inches wide and two feet long. Each platelet was crimped along its axis such that the 3/8 inch outside diameter copper tubes snapped snuggly into position. A General Electric bonding cream (Silicone Insulgrease G-624) was used for the bonding material to eliminate airspace and enhance heat transfer through the bond.

The twelve parallel tubes were connected at each end to a 7/8 inch diameter copper header. It will be shown later that the header size should be larger for flow considerations. The tubes also had turbulators inside all along the four foot length. They were constructed of 1/4 inch wide, .025 inch thick strips of brass with a 180 degree twist every inch.

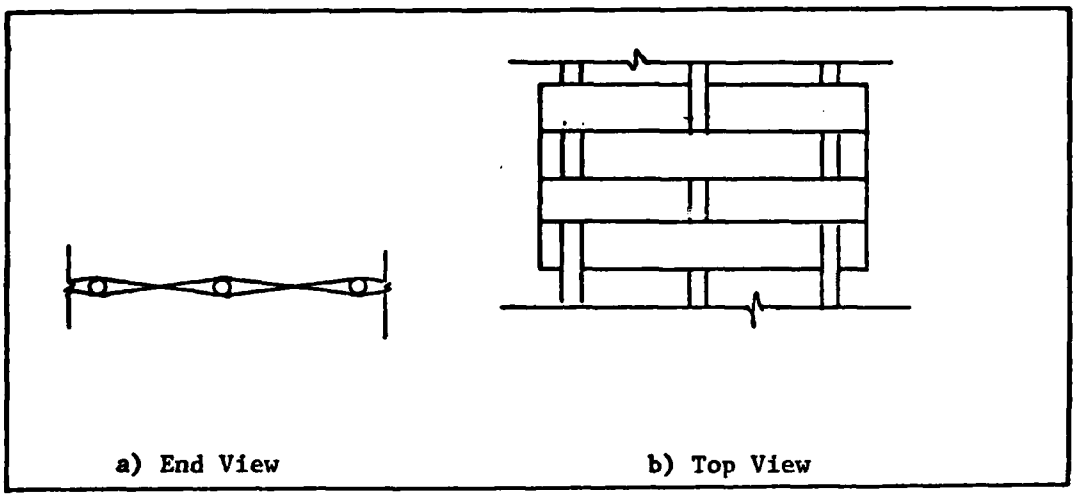

Figure 2 Schematic of the Woven Fin Configuration

The overall dimensions of the frame were 6 1/2 X 55 1/2 X 51 1/2 inches. The back side of the frame was constructed of 1/4 inch plywood with the remainder made of 3/4 inch thick pine board. There were two partially transparent Kalwall Sunlite covers spaced 3/4 inches apart and 3/4 inch separation between the second cover and the absorber plate. Below the absorber plate 3 1/2 inches of fiberglass insulation with the paper side up was installed to reduce heat loss.

The copper coated platelets which made up the absorber plate were coated with a Nextel 3M 101-10C highly absorbing flat black paint often used in solar collectors. Refer to reference 5 for a more complete description.

An alternate configuration of the absorber plate was also examined. It consisted of six inch wide strips of .028 inch thick AISI 1006 steel. Each strip was 50 inches long. A total of eight strips were required to construct the alternate plate. Each six inch strip was alternately woven between the tubes to increase contact pressure and hence bond conductance between the fin and tube. Figure 2 is a schematic of the woven fin plate.

Energy Balance Equation and Derivation

The equation defining the useful energy gain of a flat plate collector is a steady state equation which can be expressed in a variety of forms. In its most simple and useful form (Ref 2:125) it is written as:

$$Q_u = A_c F_R \left[I(\overline{\tau\alpha}) - U_L(t_{fi} - t_\infty) \right] \quad (1)$$

where
- A_c = collector area
- F_R = heat removal factor
- t_∞ = ambient temperature
- U_L = overall loss coefficient (plate to ambient)
- t_{fi} = inlet fluid temperature
- I = solar insolation (beam and diffuse)
- $(\overline{\tau\alpha})$ = effective transmittance-absorptance product.

The solar insolation may be either measured or predicted, but since this quantity is usually subject to considerable variability due to local weather and pollution conditions, a long term average hourly value is usually used. If the collector is tilted I changes accordingly. The effective transmittance-absorptance product accounts for reflected and absorbed radiation of the cover system, the absorption of the absorber plate, reduced energy losses of the collector due to cover temperature increases when radiation is absorbed, and dirt and shading factors.

A number of simplifying assumptions are employed for the determination of the factors appearing in Eq (1). The most important of these are:

(1) Steady state performance

(2) Uniform flow

(3) One dimensional heat flow through the back, covers, and edges

(4) Heat losses through the front, back and edges are to the same ambient temperature

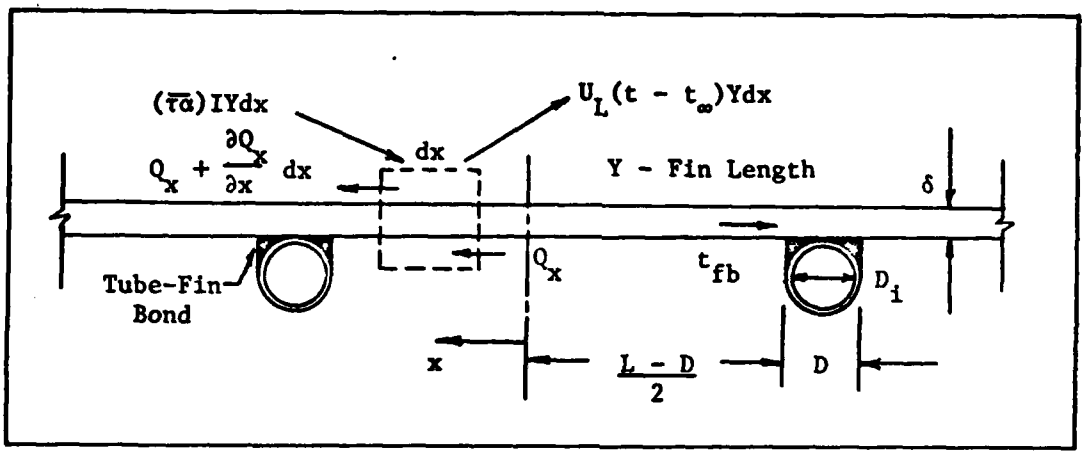

Figure 3 Absorber Plate and Tube Dimensions

(5) Temperature gradients in the direction of flow and between tubes can be treated independently.

A more complete description of the assumptions is given by Duffie and Beckman (Ref 2:125).

With these assumptions in mind, the development of the collector equation proceeds through several stages starting with an energy balance on the absorber plate fin. A negligible temperature gradient in the flow direction is also assumed. The fin is represented as in Figure 3.

Writing an energy balance for the differential element of Figure 3 and employing Fourier's law of heat conduction with appropriate boundary conditions, the temperature gradient along the x direction of the fin can be obtained. Using this result, again employing Fourier's law at the fin base, and adding a term for the energy absorbed directly by the tube, the useful energy gain can be described as:

$$Q_u = nY\left[D + (L - D)F\right]\left[(\overline{\tau\alpha})I - U_L(t_{fb} - t_\infty)\right] \qquad (2)$$

where n = number of tubes

Y = fin length

F = fin efficiency = $\dfrac{\tanh\left[(U_L/k\delta)^{.5}(L - D)/2\right]}{(U_L/k\delta)^{.5}(L - D)/2}$

The energy from Eq (2) delivered at the fin base must negotiate the bond and tube internal heat transfer resistances before arrival at the fluid. Neglecting the tube wall resistance and using C_b from Appendix C, the overall resistance may be written as

$$R_i' = \frac{L}{h_i \pi D_i} + \frac{L}{C_b} \tag{3}$$

It is desirable to write the collector equation in terms of measurable quantities such as the fluid inlet temperature, t_{fi}, as opposed to the fin base temperature, t_{fb}. Using a local fluid bulk temperature, t_f, for the moment it can be shown that

$$Q_u = nYLF'\left[(\overline{\tau\alpha})I - U_L(t_f - t_\infty)\right] \tag{4}$$

where

$$LF' = \frac{1/U_L}{\frac{1}{U_L\left[D + (L - D)F\right]} + \frac{1}{C_b} + \frac{1}{\pi D_i h_i}}$$

F' is called the collector efficiency factor. The remainder of the derivation proceeds assuming the fluid bulk temperature varies exponentially along the tube. Writing the energy balance for the differential tube element shown in Figure 4, it is easy to show that the temperature varies according to

$$\frac{t - t_\infty - (\overline{\tau\alpha})I/U_L}{t_{fi} - t_\infty - (\overline{\tau\alpha})I/U_L} = \exp(-U_L LF'y/WC_p) \tag{5}$$

The final form of the collector equation is obtained by equating the actual energy gain of the collector as measured by the inlet and outlet temperatures and the total mass flowrate to the gain the collector would

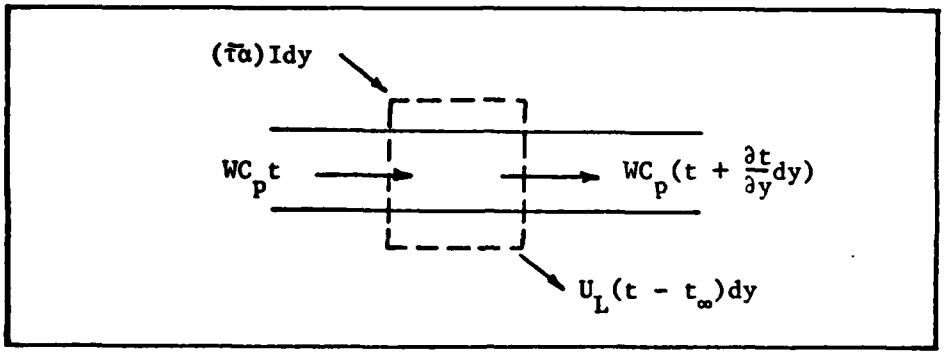

Figure 4 Energy Balance on the Tube Fluid Element

see if the absorber plate were at the fluid inlet temperature. We also employ Eq (5) at y = Y:

$$Q_u = A_c F_R\left[(\overline{\tau\alpha})I - U_L(t_{fi} - t_\infty)\right]$$

where

$$F_R = \frac{WC_p}{A_c U_L}\left[1 - \exp(-U_L A_c F'/WC_p)\right] \qquad (6)$$

F_R = collector heat removal factor.

With this equation the useful energy gain of the collector is conveniently expressed in terms of the known inlet fluid temperature. But as a consequence of using the inlet fluid temperature, the term describing the collector losses in Eq (1) decreased since t_{fi} is smaller than the effective absorber plate temperature. The effect of F_R is to compensate for this decrease by reducing the net useful energy gain of the collector from its value using t_{fi} to what it actually is using a fluid temperature that increases in the flow direction.

As seen by Eq (6), F_R is a function of three variables (F', U_L, and W). The dependency, however, is weak for all except the mass flowrate, W. So in the limit as the flow approaches a large number, where the difference

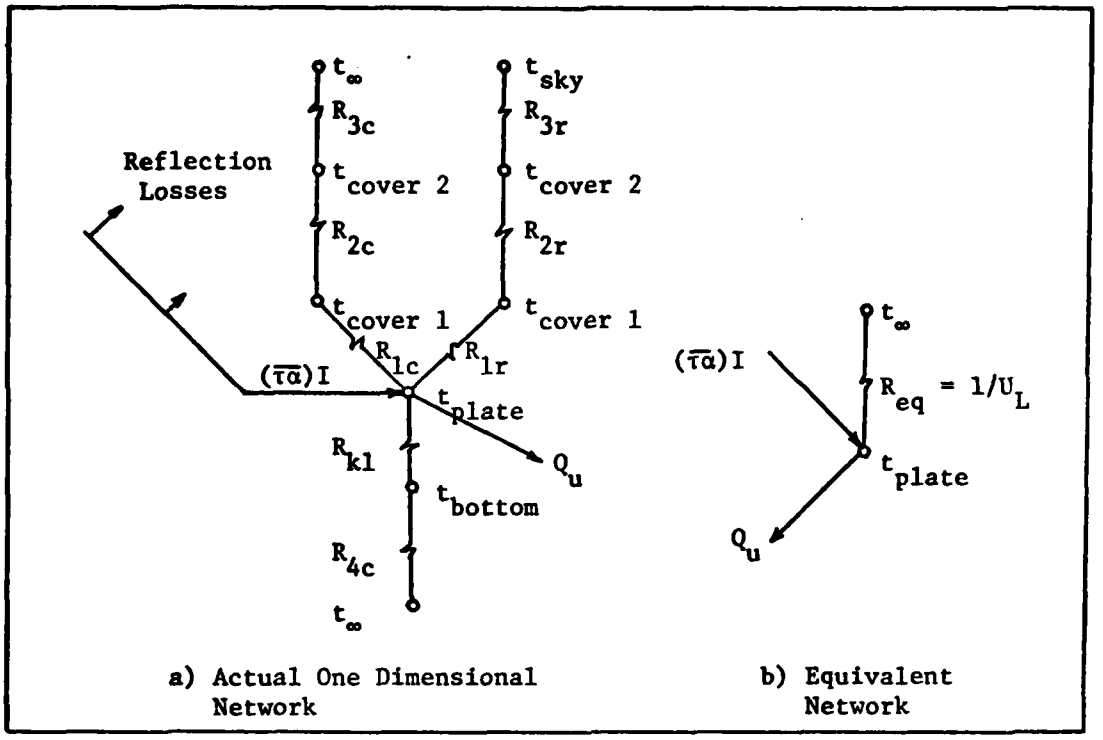

Figure 5 Thermal Network Representing the Flat Plate Collector

between the inlet fluid temperature and the mean plate temperature approaches zero, there is no required compensation. Under this condition F_R approaches, but does not surpass, the numerical value of the collector efficiency factor. However, as the flowrate decreases, the mean plate temperature and inlet fluid temperature difference increase; collector losses decrease and compensation is required. F_R is reduced accordingly for this situation.

Collector Overall Loss Coefficient

The overall loss coefficient appearing in Eq (1) can easily be evaluated by employing classical techniques. Since it is desirable to develop this concept to simplify mathmatics, consider the thermal network of a two cover system shown in Figure 5.

Figure 5 illustrates the simplicity of the heat transfer process when one dimensional heat flow is assumed. In reality three dimensional temperature gradients exist, but as the collector area increases these effects become secondary-allowing the one dimensional heat flow assumption.

Some of the incident radiation, I, is lost by reflection from the covers. The portion that finally is absorbed by the plate is the product of the effective transmittance-absorptance product ($\overline{\tau\alpha}$) and I. The portion that is lost occurs by all three modes of heat transfer. Resistances R_{1c} thru R_{4c} are convection resistances. R_{1r} thru R_{3r} are radiation resistances. This path represents heat lost from the plate to ambient by sucessive radiation from one cover to the next, etc. A third path is radiation from the plate directly to the sky considering the long wavelength transmittance of the cover system. If the cover system is opaque, zero heat loss will occur through this path. Conduction and convection losses out the back side of the collector are also shown by the path containing R_{k1} and R_{4c}.

After computing the numerical values of the resistances the entire network can be simplified to the equivalent network shown in Figure 5b.

The relative magnitude of the loss terms for the convection and radiation paths is a function of the plate emissivity and the number of covers. Duffie and Beckman (Ref 2:131) summarized these two heat transfer modes for a couple of configurations. Results are reproduced in Figure 6 and show that depending on the collector both radiation and convection losses can be significant.

The calculation of the overall heat loss is necessarily an iterative process but requires only one to two iterations at most. Klien (Ref 3)

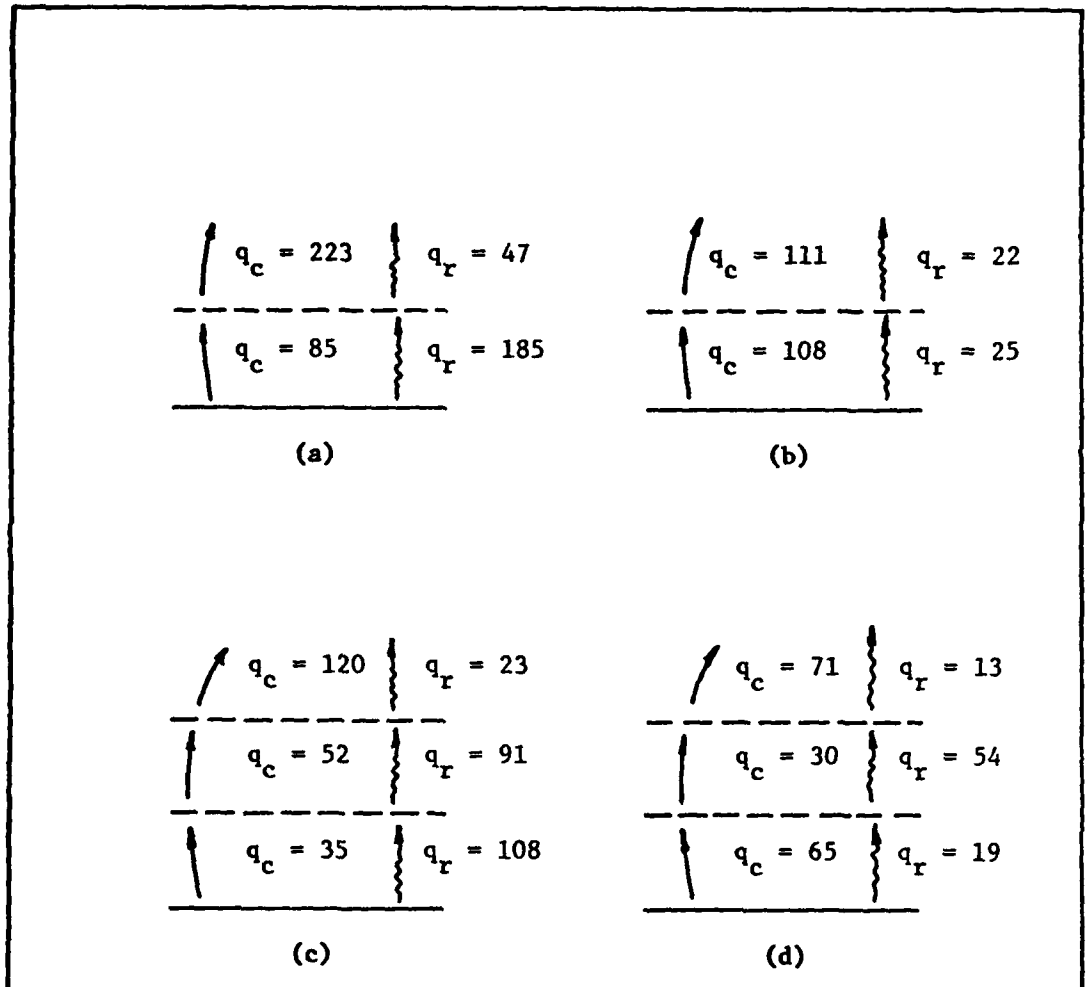

(a) One Cover, Plate Emittance = .95
U_L = 1.426 B/hr-ft^2-F

(b) One Cover, Plate Emittance = .1,
U_L = .7046

(c) Two Covers, Plate Emittance = .95,
U_L = .757

(d) Two Covers, Plate Emittance = .1,
U_L = .44

(Ref 2:131)

Figure 6 Convection and Radiation Loss Terms for Plate Temperatures of 212 F, Ambient and Sky Temperature of 50 F, Plate Spacing of 1 inch, 45 Tilt and Wind Speed of 16.4 ft/sec (All heat flux terms in B/hr-ft^2)

developed an empirical relationship to compute the top loss coefficient as a function of mean plate temperature. It greatly simplifies the otherwise iterative techniques required. It appears below for convenience as derived for a tilt angle of 45 degrees:

$$U_t(45) = \left[\frac{N}{(344/T_p)\left[(T_p - T_a)/(N + f)\right]^{.31}} + \frac{1}{h_w}\right]^{-1} + \frac{\sigma (T_p + T_a)(T_p^2 + T_a^2)}{\left[\epsilon_p + .0425N(1 - \epsilon_p)\right]^{-1} + \left[(2N + f - 1)/\epsilon_g\right] - N} \quad (7)$$

The coefficient as a function of tilt angle S is then

$$U_t(S) = U_t(45)\left[1 - (S - 45)(.00259 - .00144\epsilon_p)\right] \quad (8)$$

where
- N = number of covers
- $f = (1 - .4h_w + 5X10^{-4}h_w)(1 + .058N)$
- ϵ_g = emittance of glass covers
- ϵ_p = plate emittance
- T_a = ambient temperature (deg K)
- T_p = plate temperature (deg K)
- $h_w = 5.7 + 3.8V$ (W/m^2C)
- V = wind velocity (m/sec)

A complete analytical treatment of the overall loss coefficient is given in Appendix D.

Mean Plate Temperature

The overall loss coefficient, U_L, is based on a mean plate temperature. To arrive at an expression for the mean plate temperature in terms of measurable quantities, Eq (5) is integrated over the length of the tube to obtain a mean fluid temperature:

$$t_{fm} = \frac{1}{Y}\int_0^Y t(y)dy \tag{9}$$

Using the heat removal factor, Eq (1), and performing the integration, Klein (Ref 3) showed that the mean fluid temperature is given by

$$t_{fm} = t_{fi} + \frac{Q_u/A_c}{U_L F_R}\left[1 - \frac{F_R}{F'}\right] \tag{10}$$

Strictly speaking the temperature difference between the fluid and the tube will not be constant, but in certain cases this condition is approached. Therefore, the mean fluid temperature and mean plate temperature are approximately related by

$$t_{pm} - t_{fm} = Q_u R_{pf} \tag{11}$$

where R_{pf} is the heat transfer resistance between the plate and the fluid.

III Internal Heat Transfer Coefficient Test

The design of flat plate solar collectors was greatly simplified and assisted with the evolution of Eq (1) and the corresponding plate-fin efficiency, collector efficiency and the heat removal factors. Many of the related parameters are geometrical in character and can be accurately defined. The internal heat transfer coefficient, however, is much more difficult to assess with certainty, but its effect on the collector efficiency factor can easily be demonstrated.

Neglecting the tube wall resistance the expression for the collector efficiency factor of the fin and tube flat plate solar collector from Eq (4) is

$$F' = \frac{1/U_L}{L\left[\frac{1}{U_L\left[D + (L - D)F\right]} + \frac{1}{C_b} + \frac{1}{\pi D_i h_i}\right]}$$

Assuming, C_b = 18.88 B/hr-ft-F, 1.57 B/hr-ft-F
U_L = .65 B/hr-ft^2-F, 1.3 B/hr-ft^2-F
δ = .035 inch
L = 4 inch
D = 7/16 inch
D_i = 5/16 inch
k = 26 B/hr-ft-F

the dependence of the collector efficiency factor, F', on the internal heat transfer coefficient can be shown as in Figure 7. Two overall loss coefficients and two values of bond conductance have been included as parameters. The loss coefficient of .65 B/hr-ft^2-F is the nominal value for the two cover configuration. Elimination of one of the Kalwall covers nearly doubles the loss coefficient, so a value of 1.3 B/hr-ft^2-F was also

plotted. The two bond conductances are the experimentally determined average values for the clamped fin and tube and the woven fin and tube respectively.

Figure 7 shows there is no significant improvement in the collector efficiency factor for internal heat transfer coefficients greater than 50 B/hr-ft^2-F. Additionally, computations can show that a 10 percent error in h_i of this order of magnitude produces only about a one percent change in F', so extreme accuracy in the estimation of h_i in this range is not essential either.

The functional dependence of the bond conductance also shown in Figure 7 has been shown by Whillier (Ref 16:96). That data shows improvements in bond conductance beyond about 20 B/hr-ft-F are questionable considering the implementation troubles likely to be encountered trying to exceed this amount.

Therefore, from these considerations it would seem there is little necessity to design a collector with bond conductances and internal heat transfer coefficients exceeding 20 B/hr-ft-F and 50 B/hr-ft^2-F respectively. Nevertheless, tests were conducted in order to assess the actual values for different configurations.

Test Description and Procedure

Figure 8 depicts the experimental test set up for determination of the internal heat transfer coefficient. Details of the tube-fin are shown in Figure 9.

Wadding was used at both the inlet and exit of the tube to promote fluid mixing and obtain true bulk temperature measurements with thermocouples T1 and T10. Thermocouples T2 thru T8 were soldered to the underside of the tube and equally spaced along the length. The submersible

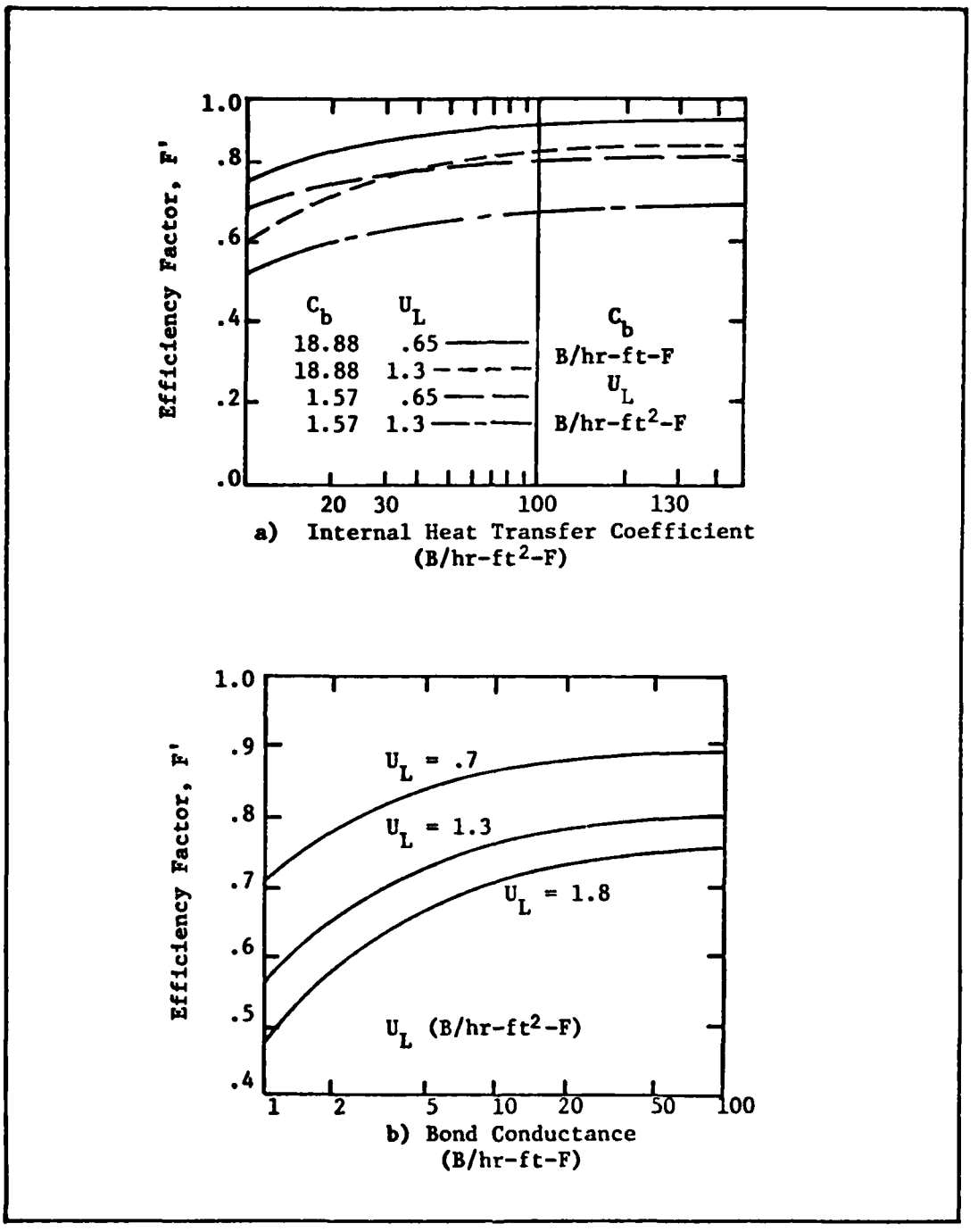

(Ref 16:96)

Figure 7 Effect of the Internal Heat Transfer Coefficient and Bond Conductance on the Collector Efficiency Factor

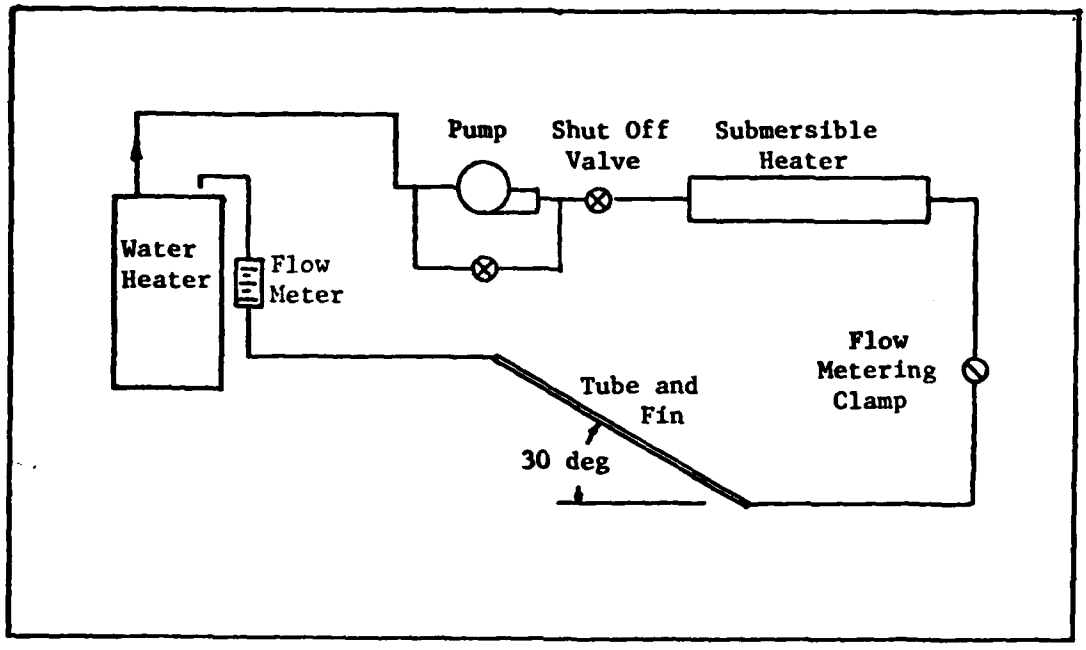

Figure 8 Test Apparatus for the Internal Heat Transfer Coefficient Test

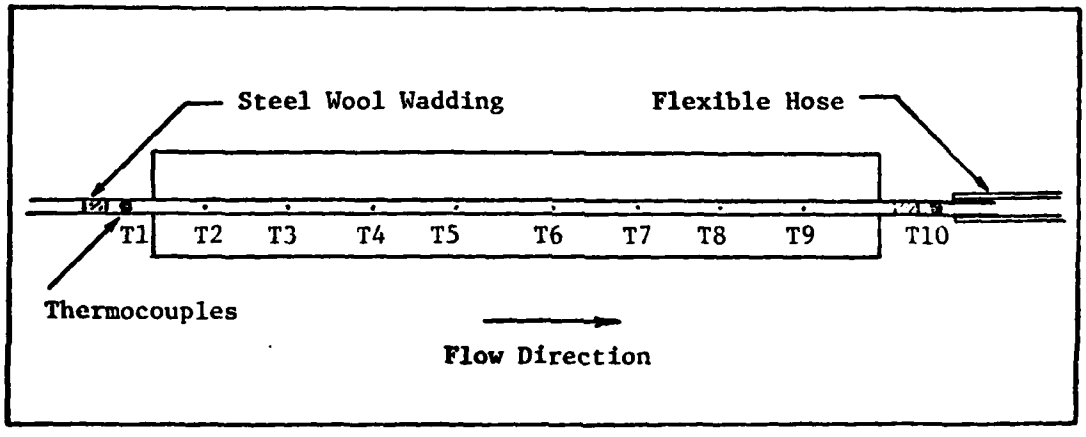

Figure 9 Heat Transfer Coefficient Test Specimen

heater provided heat input to replace that lost during circulation. Metering clamps and flow meter were used for flow adjustments. Actual flowrates were measured using a pan, scales, and timer. The recommended collector flowrate (Ref 5) is about 3.3 lbm/min which is equivalent to 16.5 lbm/hr/tube, so the experiment was conducted for flowrates between 4.64 lbm/hr and 20.94 lbm/hr. Steady conditions were obtained for each reading, but the inlet fluid temperature, T1, varied between 131-159 F depending on the flowrate. A summary of the data taken is given in Appendix A.

The test was conducted by first heating the water while it was being circulated to facilitate equilibrium conditions. The water heater was thermostatically set at or near 145 F for automatic shut off. However, with the submersible heater steady temperatures as high as 159 F were obtained for some readings. After heating, the flowrates were set at small values first, and the system was allowed to run until temperatures reached equilibrium. Once equilibrium was achieved temperature measurements and flowrates were recorded. The system was then set to another flowrate. The test was conducted twice-with and without turbulators. Both times the hot water was pumped up from the bottom of the tube and fin.

Results

To compute the local Nusselt number it is necessary to obtain the local bulk temperature. Because of the small diameter tubes it was not possible to measure this quantity, so recourse was made to predicting it. Under high flowrate conditions the bulk temperature will almost vary linearly along the tube, but strictly speaking it is more nearly approximated by an exponential function. Assuming the fin overall loss

coefficient remains constant the bulk temperature is given by

$$t_f(x) = (t_{fi} - t_\infty)\exp(-ULx/WC_p) + t_\infty \qquad (12)$$

The local Nusselt number was computed by

$$Nu_x = \frac{UL\left[t_\infty - t_f(x)\right]}{k\pi Y\left[t_w(x) - t_f(x)\right]} \qquad (13)$$

where
- W = mass flowrate
- U = fin loss coefficient
- L = fin width
- t_∞ = ambient temperature
- $t_f(x)$ = local fluid temperature
- $t_w(x)$ = local wall temperature
- k = thermal conductivity
- Y = tube length
- t_{fi} = inlet fluid temperature.

The derivation of these expressions is given in Appendix A.

Figures 10 and 11 plot the measured wall temperature and computed bulk temperatures for the lowest flowrate conditions. Since the bulk and wall temperatures vary the most along the tube under low flow conditions the plots serve as an indication of the validity of a linear bulk temperature variation assumption. Figure 10 which is the tube with turbulator shows that a linear assumption is probably not adequate under low flow conditions. But at higher flowrates the bulk temperature variation will become more linear. In contrast Figure 11 shows that the linear assumption when turbulators are not present is not too bad even for the lowest flowrate condition. From this consideration alone it appears the turbulators have a significant influence on the heat transfer characteristics.

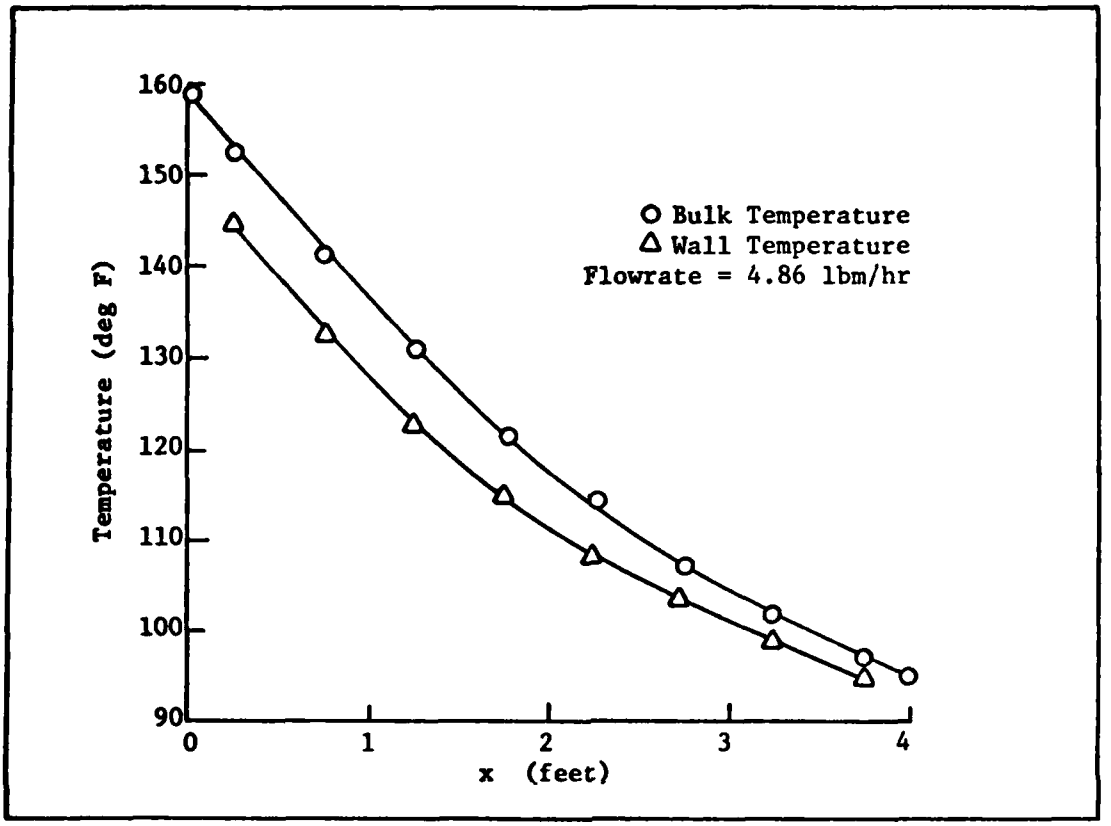

Figure 10 Wall and Fluid Bulk Temperatures Along the Tube With Turbulators

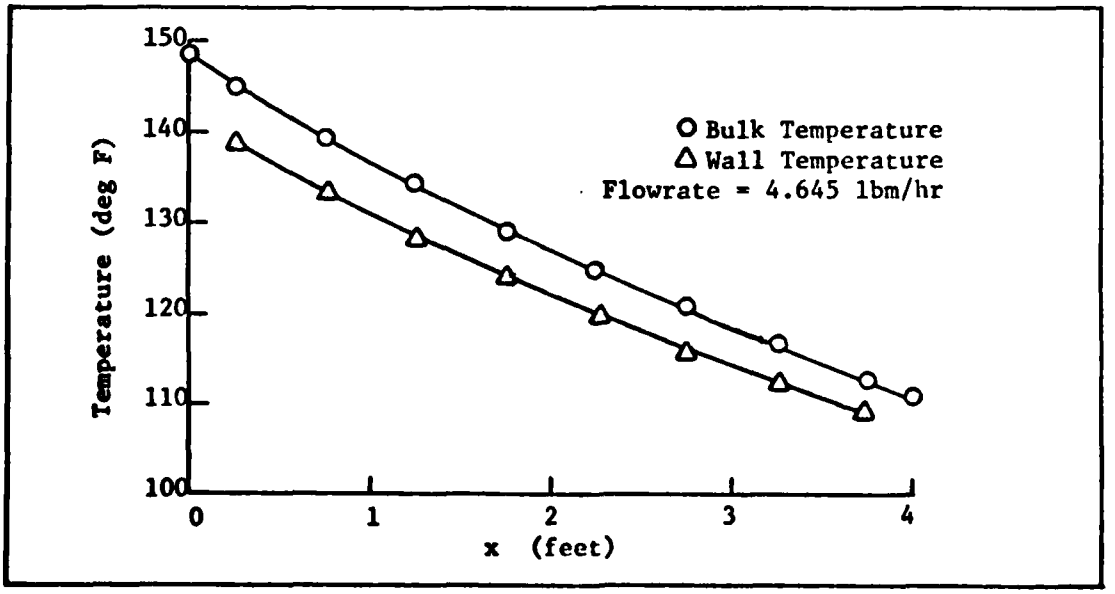

Figure 11 Wall and Fluid Bulk Temperatures Along the Tube Without Turbulators

The Reynolds number varied between 100 and 1600 for the entire test so the flow condition would appear to be laminar over the entire range. But a plot of the local Nusselt numbers shown in Figure 12 does not substantiate this conclusion even without the turbulators. With the use of turbulators mean Nusselt numbers increased significantly with flowrate, and local values increased in the flow direction-except for the lowest flowrate condition. Without turbulators mean Nusselt numbers increased only marginally with increasing flow. Local values were fairly constant over the length except at the ends where increasing values were noted.

Under laminar flow theory given by Kays (Ref 7:102-145) which neglects free convection effects, a reduction in the local Nusselt number occurs along the flow direction until fully developed velocity and temperature profiles result. Then the local Nusselt number remains constant. Since this condition was not typical of the results shown in Figure 12, it was suspected that significant free convection effects were present.

This seems to be especially evident for the tubes without turbulators for three reasons. First, the Nusselt numbers are nearly constant along the length of the tube but at a higher value than 4.34 which theory prescribes for a constant heat flux solution. Secondly, the Nusselt number increases slightly over the last half of the tube-an effect which occurs only with increased mixing action. Thirdly, at the highest flowrate of 20.94 lbm/hr the local values begin to behave according to theory by dropping off during the first half of the tube-as though free convection was not significant.

With turbulators the Nusselt numbers were much higher-ranging from 10 to as high as 20. And, since the local values increased in the flow

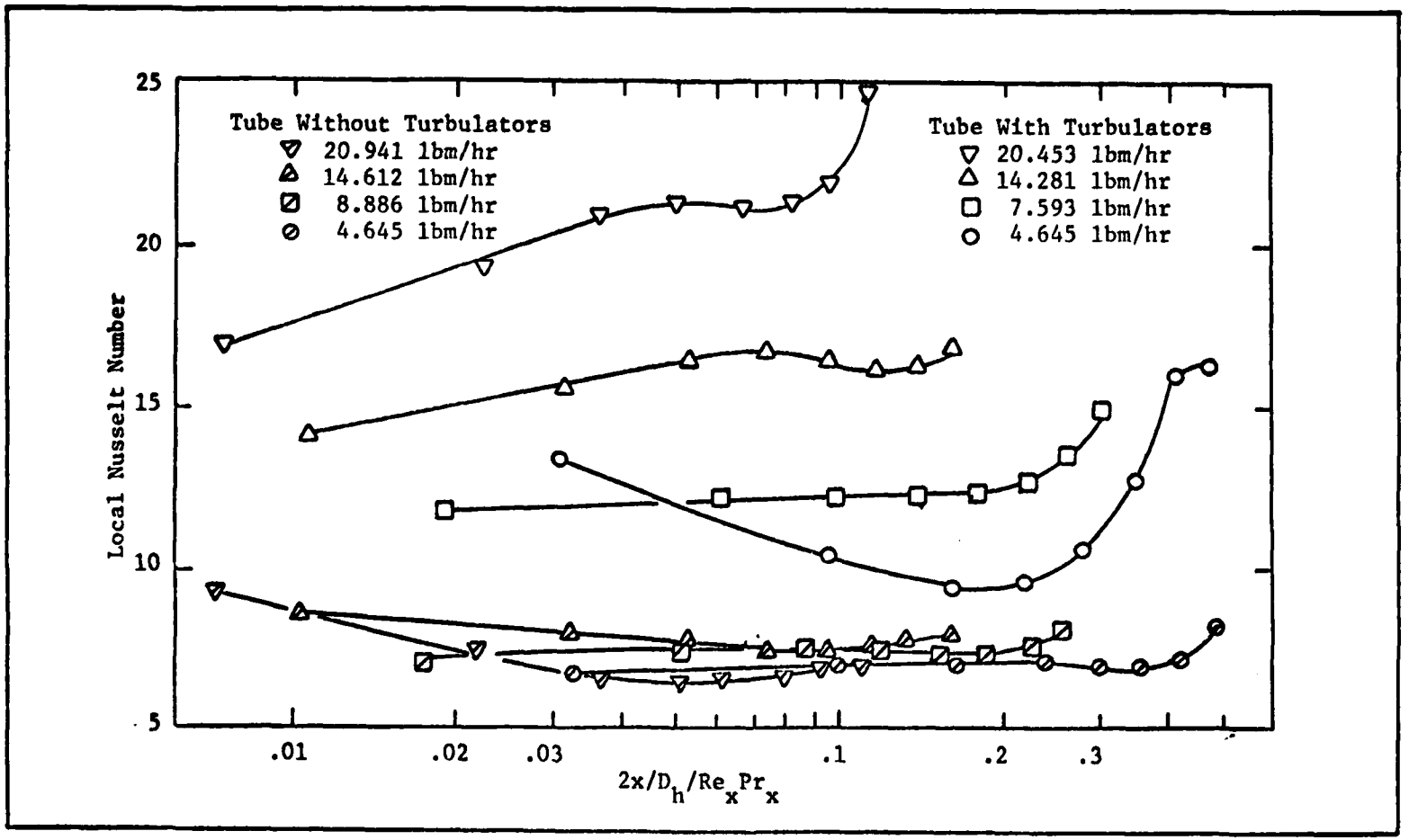

Figure 12 Local Nusselt Number Variation for a 30° Inclined Tube with a Clamped Fin Based on an Exponential Bulk Temperature Decrease

direction for all but the lowest flowrate, it was evident that the flow was turbulent inspite of the low Reynolds numbers. It appears that momentum changes induced by the twisting action of the turbulators coupled with any natural convection forces present helps promote early transition and increasingly turbulent flow behavior.

Discussion

An order of magnitude analysis of the boundary layer (Ref 10:357-358) helps to put the relative magnitudes between free and forced convection forces into proper perspective. The result of such an analysis says free convection is significant if the ratio of Grashof to the square of Reynolds number is of the order one, i.e.,

$$Gr/Re^2 = 1 \tag{14}$$

The higher the ratio the more significant free convection becomes. For tubes with turbulators this ratio varied between .051 at the lowest flowrate to .0013 at the highest-indicating progressively weaker free convection effects with increasing flowrate. Without turbulators this ratio ranged from .805 to .043 indicating strong free convection effects for all but the highest flowrates. Based on this simple analysis it can be concluded that combined free and forced convection effects existed for the lowest flowrate conditions and probably so for the modest flowrates as well.

Heat transfer influenced by the simultaneous interaction of gravitational and other forces such as pressure gradients has been investigated by various sources in the past (Ref 8, 11, 12, 13), but a complete knowledge in this field is lacking because the direction of flow enters the problem as well as the parameters usually defining free and forced

convection separately. Additionally, all sources quoted here conducted investigations either under constant heat flux or constant wall temperature situations, so their results may not correlate well with the present study since neither situation was typical of test conditions.

The literature does indicate however that transition can be expected to occur much more rapidly under low Reynolds number conditions with heat transfer than isothermal or adiabatic flow. For instance, experimental work by Kemeny and Somers (Ref 8:339-345) on constant heat flux vertical tubes indicated that transition took place at a Reynolds number of about 200 for water. For oil the transition was much earlier-occurring at Reynolds numbers as low as 10. Metais and Eckert (Ref 12:295-298) conducted a survey and summarized a portion of the available literature on combined effects in 1964. That summary is given for vertical and horizontal tubes in Figures 13 and 14.

Combinations of aiding and opposing flow as well as uniform heat flux (UHF) and uniform wall temperature (UWT) are shown. It is fairly easy to anticipate the results shown in these figures. A large Reynolds number implies a large forced flow velocity; the larger the value of the Grashof-Prandtl product, the more one would expect free convection effects to prevail. And of course, in between, is the mixed region where both effects are significant.

Oliver (Ref 13:335-350) studied natural convection effects on uniform wall temperature horizontal tubes and concluded that the mean Nusselt number could be satisfactorily represented by

$$Nu_m = \left[\frac{\mu_b}{\mu_w}\right]^{.14} 1.75\left[Gz_m + .0083(Gr_m Pr_m)^{.75}\right]^{1/3} \qquad (15)$$

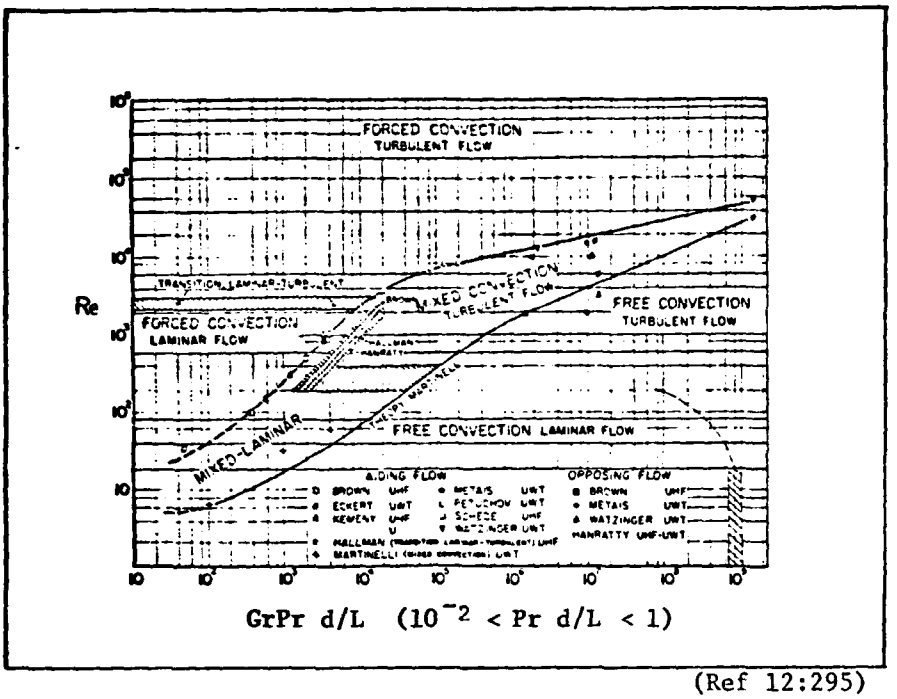

(Ref 12:295)

Figure 13 Regimes of Free, Forced, and Mixed Convection for Flow Through Vertical Tubes

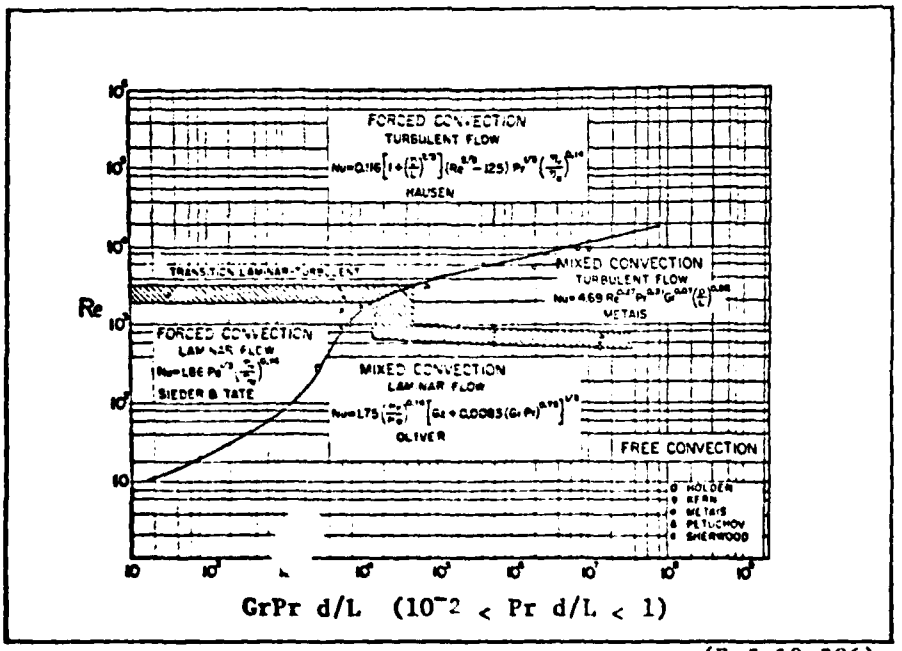

(Ref 12:296)

Figure 14 Regimes of Free, Forced, and Mixed Convection for Flow Through Horizontal Tubes

where μ_b = viscosity of fluid measured at the average of initial and final bulk values

μ_w = viscosity of fluid measured at the wall temperature

$Gz_m = WC_p/kY$

Gr_m = Grashof number based on tube diameter and difference between film temperature (the average of the wall and average bulk temperature) and wall temperature

$L/D > 70$

Provided as comments to Eckert and McComas' work on a horizontal uniform wall temperature tube (Ref 11:147-153), Thomas and Brown proposed

$$Nu = \left[\frac{\mu_b}{\mu_w}\right]^{.14} 1.75\left[Gz_m + .012(Gz_m Gr_m^{1/3})^{4/3}\right]^{1/3} \quad (16)$$

This correlation supposedly fits water data to within ± 8 percent over a range of Reynolds numbers of approximately 200-1500 together with a Grashof number range from 4×10^4 to 40×10^6 and varying L/D ratio.

Baker (Ref 1:78-85) also studied heat transfer characteristics at low Reynolds numbers (for a uniform heat flux condition) on tubes similiar to the type used in tube-in-strip collector plates. Under this type application, the temperature could be significantly higher at the fin-tube junction than at either the top or bottom of the tube. Baker concluded that this circumferential temperature variation promoted additional mixing action over and above the natural convection forces reported by (Ref 11, 13) and recommended that Eq (15) be modified by multiplication of a dimensionless temperature ratio, $\Delta t_{max}/\Delta t_{min}$ (which he failed to define), to account for it.

The results of Baker's experiment are shown in Figure 15a and b. Four local Nusselt numbers were computed along the length of the horizontal tube for fifteen flowrates. Tube wall temperatures were taken

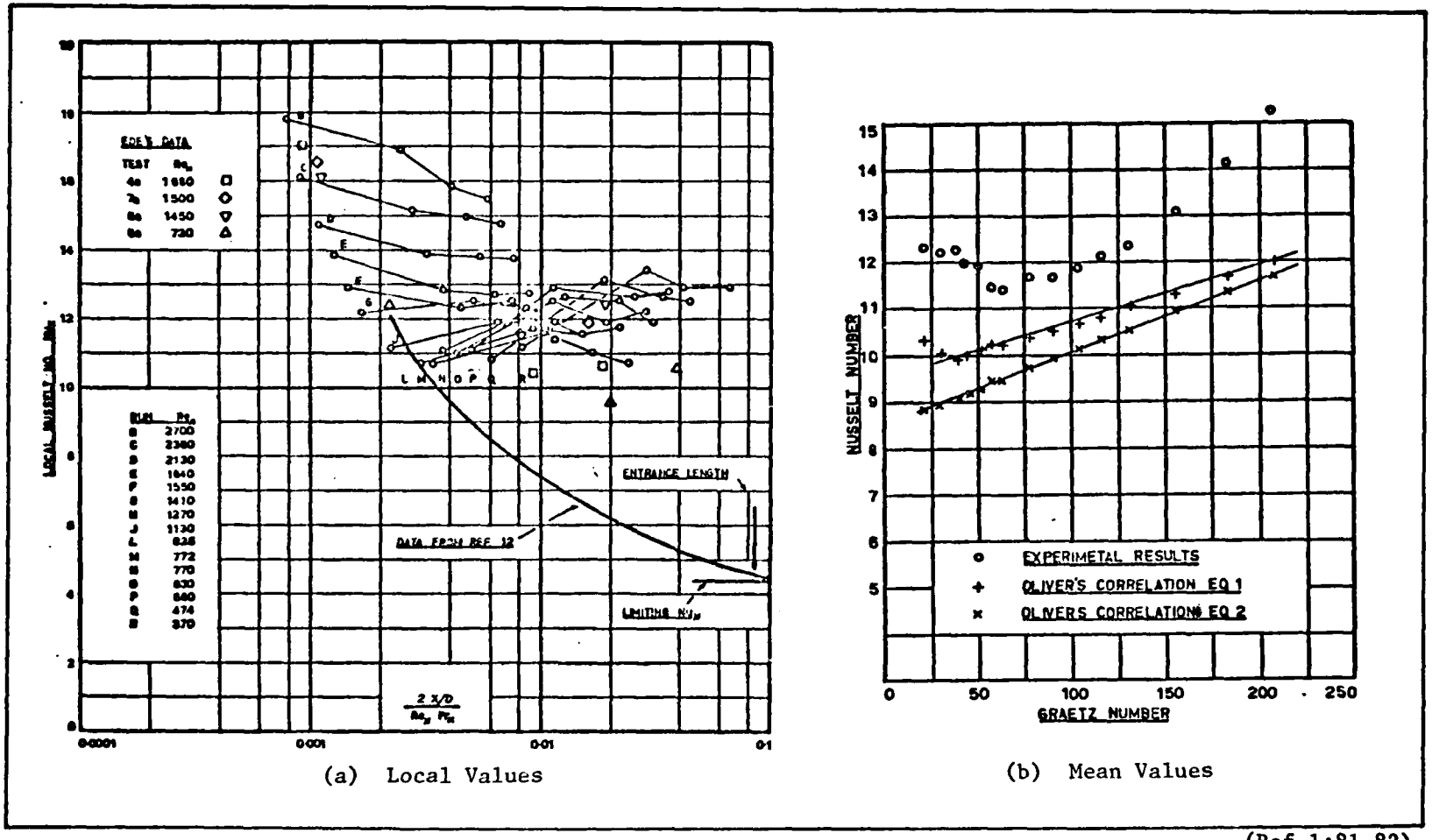

(a) Local Values

(b) Mean Values

(Ref 1:81-82)

Figure 15 Local and Mean Nusselt Numbers for a Horizontal Tube with Uniform Heat Flux

at the fin-tube junction and the fluid bulk temperature was assumed to be linear between the inlet and exit, but thermocouples were inserted into the flow field at four stations to measure local bulk temperatures for fluid property calculations.

The experimental data shown in Figure 15a is compared with a theoretical treatment given by Kays (Ref 7:102-145). Kays' treatment neglects the gravitational forces and is applicable to a constant heat flux problem only. At the higher flowrates a decrease in the local Nusselt number occurs along the tube-a condition predicted by theory neglecting gravitational forces. At lower flowrates, however, the pattern is reversed. Baker concluded that this behavior was caused by the increasing influence of gravitational forces at the lower Reynolds numbers. It appears that at the end of the tube for the low flow conditions the heat transfer reaches a fully developed condition resulting in a nearly constant Nusselt number.

Figure 15b compares the experimental arithmetic mean Nusselt number with mean values as computed by Oliver's correlations. This comparison was the basis for the proposed additional term in Oliver's equation and Baker attributed the difference to the variation of circumferential heat flux.

None of the previous work cited here really typified the test conditions since neither a constant wall temperature, constant heat flux, vertical or horizontal tube was used. The experimental mean Nusselt numbers have, nonetheless, been compared to Oliver's correlation, Eq (15), and that of Thomas and Brown, Eq (16). Comparisons could not be made with Baker's correlation since his recommended temperature ratio was not defined. The comparison was made with and without turbulators in

Figure 16. The experimental results were obtained as an arithmetic average of the local values. Correlation equations were calculated with arithmetic mean values of Grashof, Prandtl, and Gratz numbers.

As expected no correlation existed for the tubes with turbulators since this test set up did not typify past work. Results did correlate well without the turbulators, however, inspite of a non-uniform wall temperature and inclined tube. What is more important, as far as the application to the solar collector, is the resulting value of the internal heat transfer coefficient. It turns out that the minimum mean value of the internal heat transfer coefficient is 98 $B/hr\text{-}ft^2\text{-}F$ for water at 150 F. This is clearly an acceptable value considering the results presented in Figure 7. So it must be concluded that the turbulators provide only marginal improvement in the thermal performance of the collector.

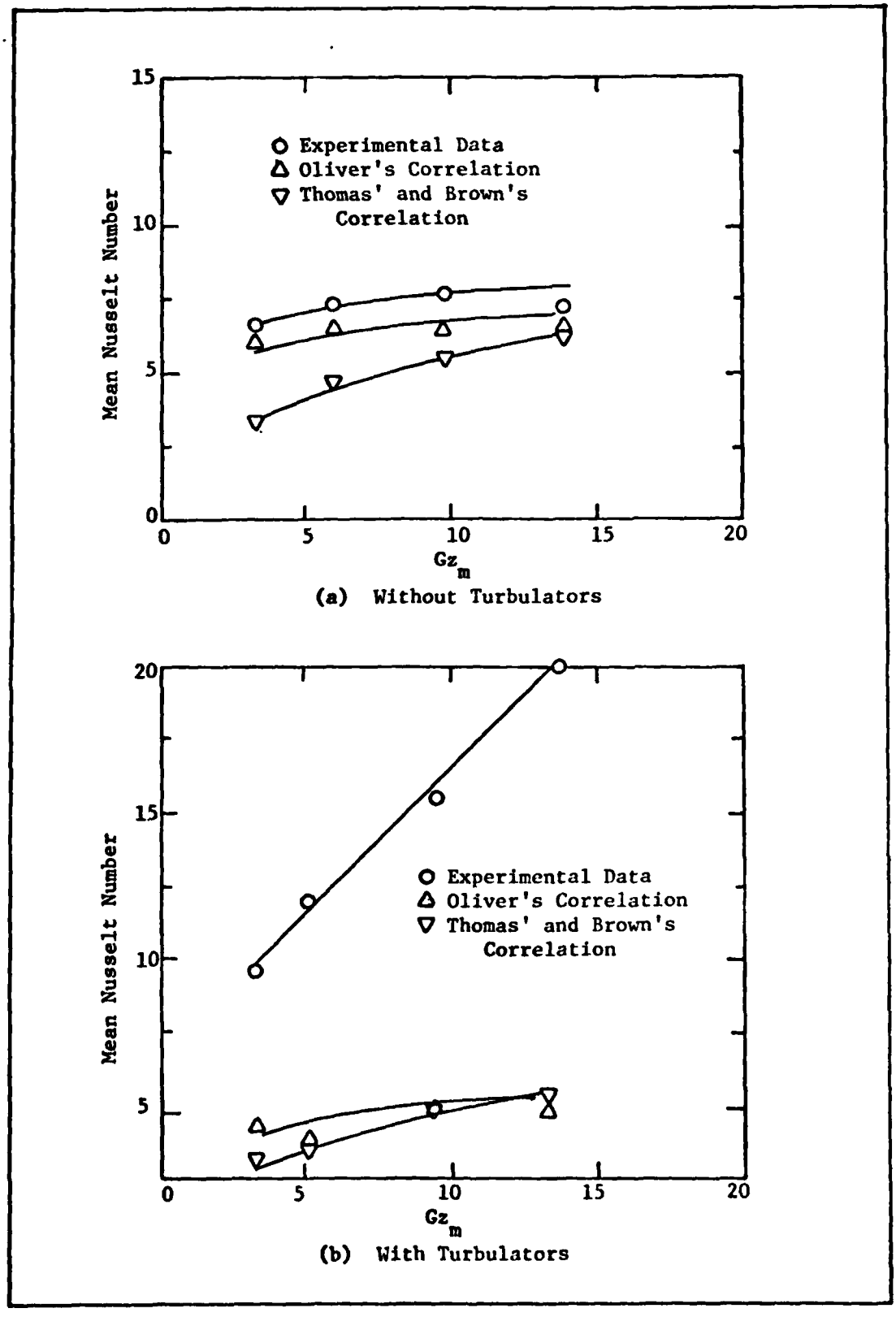

Figure 16 Experimental Mean Nusselt Numbers Compared to Correlations by Oliver and that of Thomas and Brown

IV Flow Distribution Test

In theory the collector heat removal factor can be satisfactorily computed for the flat plate solar collector. This calculation assumes uniform flow, so the accuracy is dependent upon the actual flow condition. Therefore, the purpose of this test was to examine the real flow condition. Such a test could normally be conducted by installation of flow measuring devices directly into the lines, but small inside line diameters and flowrates rendered this approach unacceptable. Instead, an array of thermocouples was used to measure temperature differences which in turn were used to draw conclusions about the flow situation.

Test Description and Procedure

Figure 17 is a schematic of the test set up. This same set up was used for the $U_L F_R$ product test which is covered later. The collector

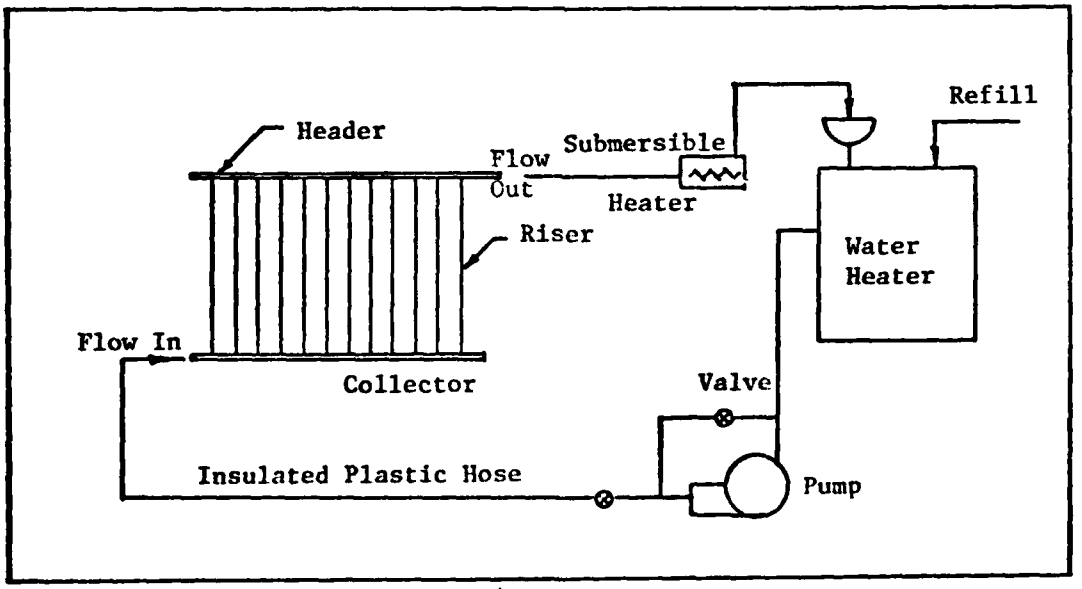

Figure 17 Test Set Up for the Flow Distribution and $U_L F_R$ Product Test

was tested at a 45 degree inclination and the liquid was circulated through an insulated plastic hose as an open loop system. This permitted flowrate measurement and control with pan, scales, and valves.

The water was initially heated to approximately 140 F with the gas fired water heater while the pump was running. The submersible heater was used to minimize temperature transients and remained on during heat up and all subsequent testing. It was possible to visualize the flow distribution by measuring the tube temperatures. For instance, if all tube temperatures were equal except one, then the flow in each tube was the same or nearly so-except for the one at a different temperature.

A study of the flow distribution was made with and without turbulators so two sets of readings were made. For both, the thermocouples were installed on the underside of the tubes mid-way between the headers, and the inlet and exit bulk temperatures were recorded. The data is listed in Appendix B.

Results with Turbulators

The test was conducted at two flowrates-2.0 and 4.125 lbm/min. The results are presented in Figure 18. The first and second independent variables are the riser number and the flowrate, respectively. The dependent variable has been defined as the difference between the riser and collector inlet temperature. Thus, as the flowrate increases the dependent variable also increases and vice versa. In addition to flow visualization, the dependent variable also permits the location of hot spots on the absorber plate.

To some degree the results of the test can be anticipated. For instance, we expect the temperature difference to decrease with increasing

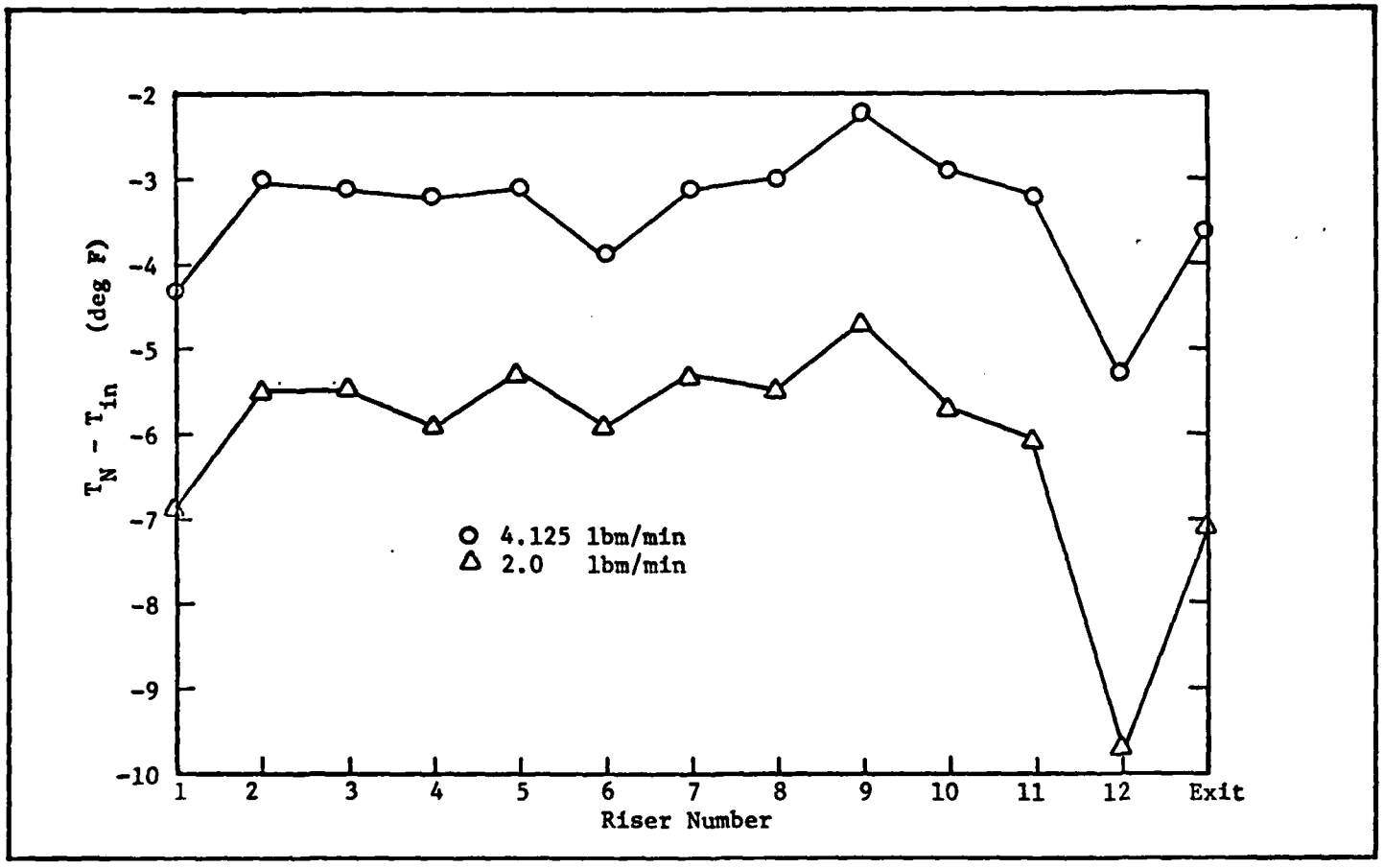

Figure 18 Flow Distribution With Turbulators as Shown by Temperature Differences for Each Riser

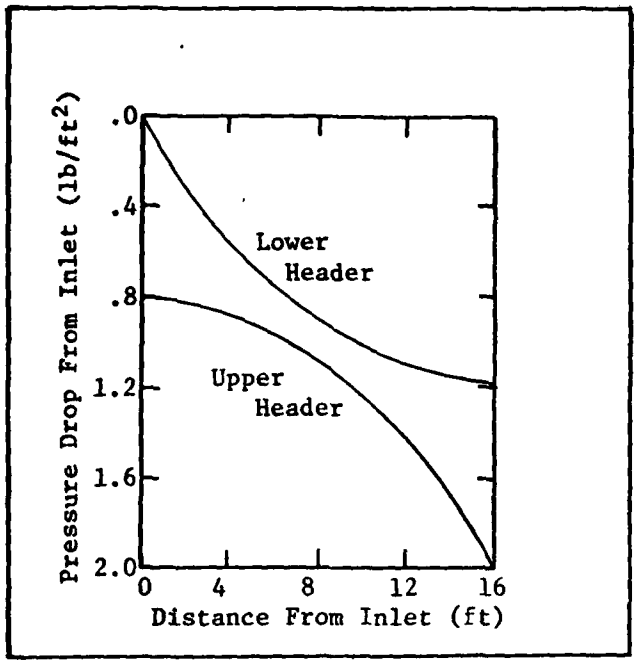

(Ref 4)

Figure 19 Calculated Pressure Distribution in Headers of an Isothermal Absorber Bank

flowrate and this happened. It was also apparent that the relative flow distribution remained the same for the two flows. This was evident by the shape of the curve. It was also evident by the large temperature differential of 9.7 F for a flow of 2.0 lbm/min, and a temperature differential of 5.3 F for the other flow, that riser number 12 had the least flow. As seen there was very little variation between the remaining tube temperatures-indicating a satisfactory flow pattern.

Dunkle and Davey (Ref 4) studied the flow distribution in parallel tubes such as this and showed that under symmetrical conditions the pressure drop situation was like that shown in Figure 19. The rate of change of pressure drop was greatest at the collector inlet for the lower header and greatest at the exit for the upper header. The rates approached one another and became equal at the center of the header. Also note that

pressure drop differences were greatest at the ends. The implication was obvious: high flow at the ends and lower flow in the center portion.

This would be the expected outcome of the data in Figure 18. Since results were not symmetrical it must be concluded that the data actually shows this particular collector's pressure drop characteristics. Furthermore, since the temperature differences were not excessive at the recommended flowrate of about 3.3 lbm/min, it was concluded that computed values of F_R were typical of the actual performance value, and that the actual flow condition was acceptable.

Results Without Turbulators

The flowrates varied from .436 lbm/min to 6.708 lbm/min while the inlet temperature was held between 123 to 138 F. Without the turbulators the results were appreciably different as Figure 20 shows. As before, the first and second independent variables were the riser number and the flowrate, respectively. Also here, the dependent variable was defined as the difference between the riser and collector inlet temperature.

The results presented in Figure 20 show a striking lack of flow uniformity. At lower flows the water simply passed through either the first or the first couple of risers. Increasing the total flow caused increasing flow in successive risers. This was evident by the decreasing temperature differential of the dependent variable. The pattern continued until 6.708 lbm/min where the temperature differentials were nearly the same-indicating more uniform flow conditions. This behavior was not indicative of the isothermal flow study conducted by Dunkle and Davey.

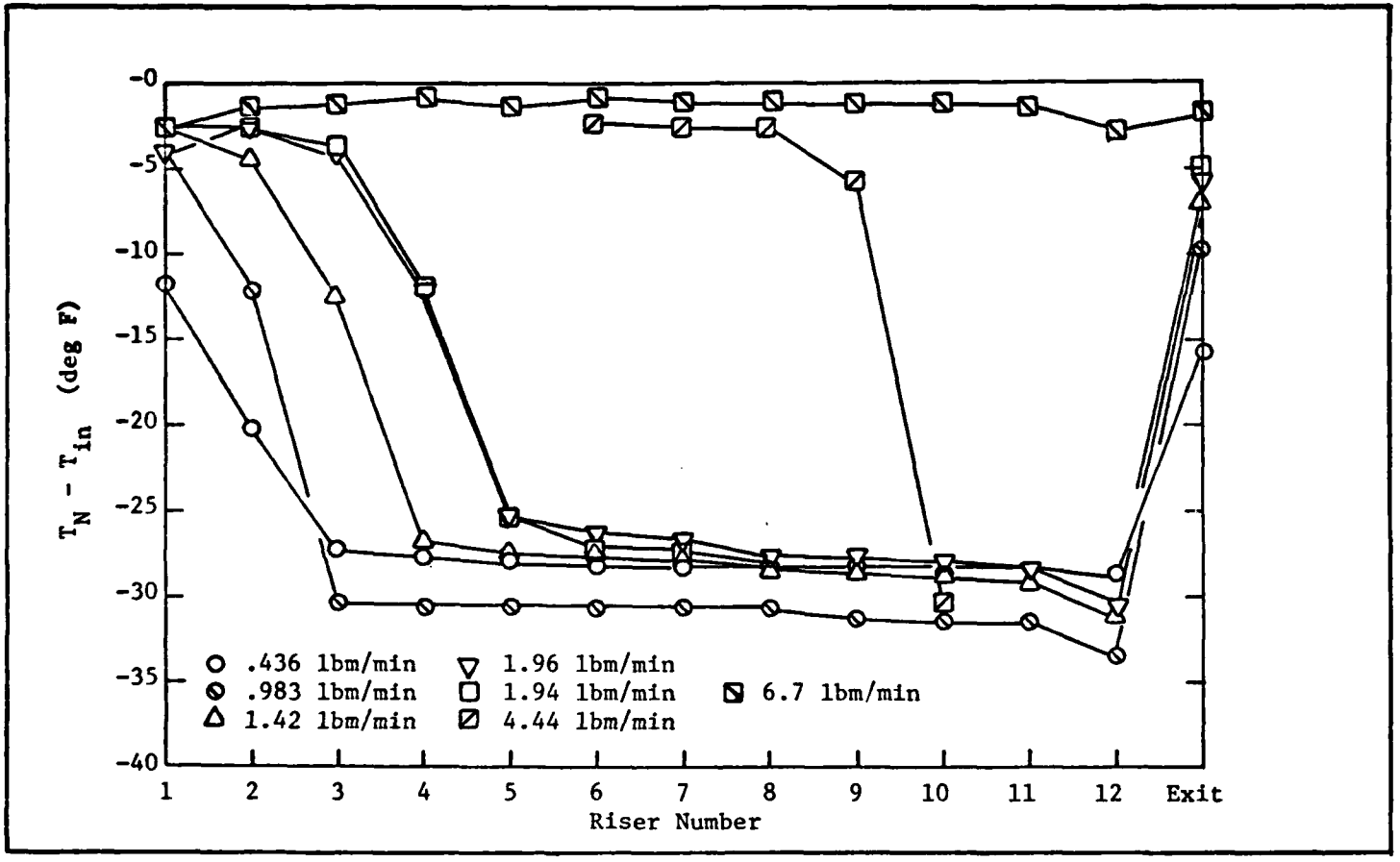

Figure 20 Flow Distribution Without Turbulators as Shown by Temperature Differences for Each Riser

Since these results were unexpected, the test was conducted a second time. Bubbles were a major source of suspicion for producing complex pressure drop characteristics, so special pains were taken to rule out their presence. This included adjusting the flowrate to the maximum and tilting the collector such that bubbles could be forced through the system. After completing this task the flowrate was reduced and the test repeated. Nevertheless, the results of the second test were still nearly identical to the first. For example, the dependent variable shown in Figure 20 for two flowrates (1.94 and 1.96 lbm/min) almost coincided for the two separate runs.

The conclusion was simple: without turbulators the flow distribution was not uniform. The explanation, however, was not simple. For instance, fluid flow calculations for an isothermal fluid like that shown in Figure 19 show that the pressure drop along the tubes near the collector inlet and exit regions become more exaggerated with increasing flow and vice versa. Consequently, on a percentage basis, more flow passes through the outer risers with respect to the center ones as total flow increases. The reverse process occurs as the flowrate is reduced. From this consideration one would expect the implied flow distribution of Figure 20 to also show an increase in flowrate in the risers farthest from the inlet under the increased flow conditons.

As clearly indicated in Figure 20, this expected effect did not occur. The flow increased very significantly in the risers nearest the inlet but did not increase at the opposite end as theory would have it. It appears another variable affecting pressure drop characteristics besides those mentioned earlier came into play. It was theorized that this pressure drop alteration came from natural convection

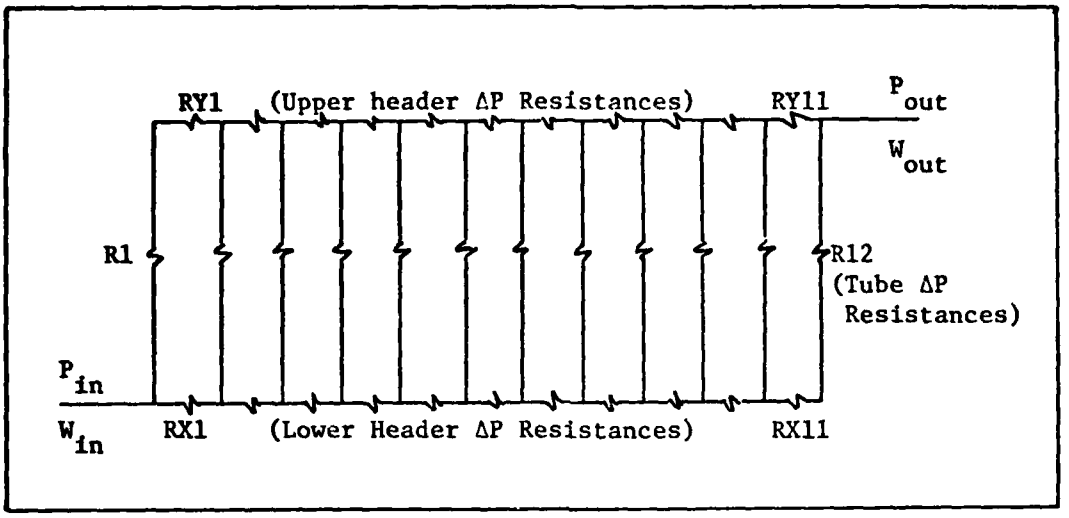

Figure 21 Isothermal Flow Network Representation of the Collector

forces described earlier. It was also noted here that the average total flow range per tube for this test was comparable to that in the internal heat transfer coefficient test, so the operating points fell well within the region of either free or mixed convection on Figure 13.

Hot water was pumped through the collector where it was subsequently cooled. It follows that if convection played a role in affecting the pressure drop, it would occur on the riser nearest the inlet because the temperature is the greatest there. As the water moves further down the headers and risers cooling takes place, temperature differentials drop, and bouyancy forces decrease. So convection becomes less important as the water proceeds along the tubes. This is illustrated by movement to the left on Figure 13. Data taken from the internal heat transfer coefficient test bear this out.

To further illustrate the condition, a pressure drop and flow evaluation model was developed by the investigator. It was designed to model the collector risers and headers for isothermal flow. Figure 21 shows

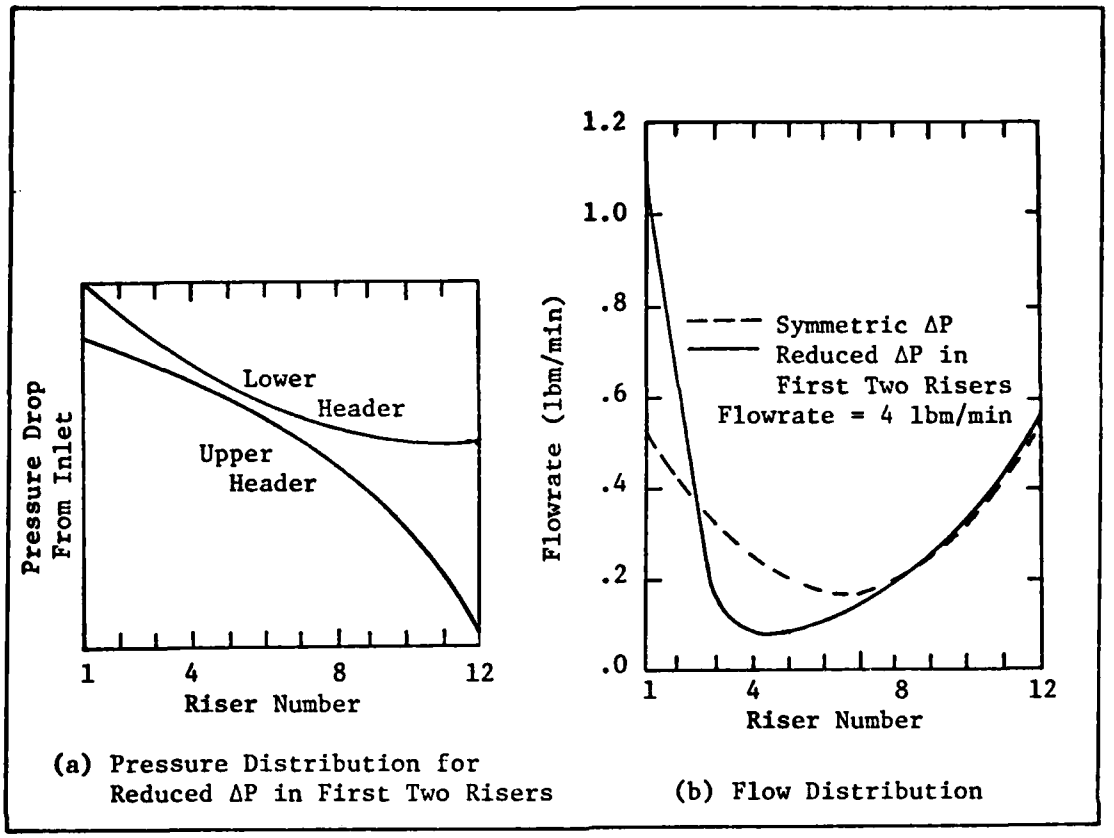

Figure 22 Flow Distribution for Symmetrical and Reduced Pressure Drop in the First Two Risers

the model network with the riser and header resistors. For specified resistor values, flowrate, and exit pressure, the flow distribution and resulting junction pressures can be obtained by the method presented in Appendix B. For the special case where the upper and lower header resistors are equal, and the riser resistors are also equal (but not necessarily equal to the header resistors), the pressures will be related as shown in Figure 19. The resulting flow distribution is shown in Figure 22. Also shown is the flow distribution for the same total flow but with reduced pressure drops in the first two risers. This was intended to simulate the effect of free convection aiding the flow. When the pressure drop was reduced in the first two risers there was a striking similarity

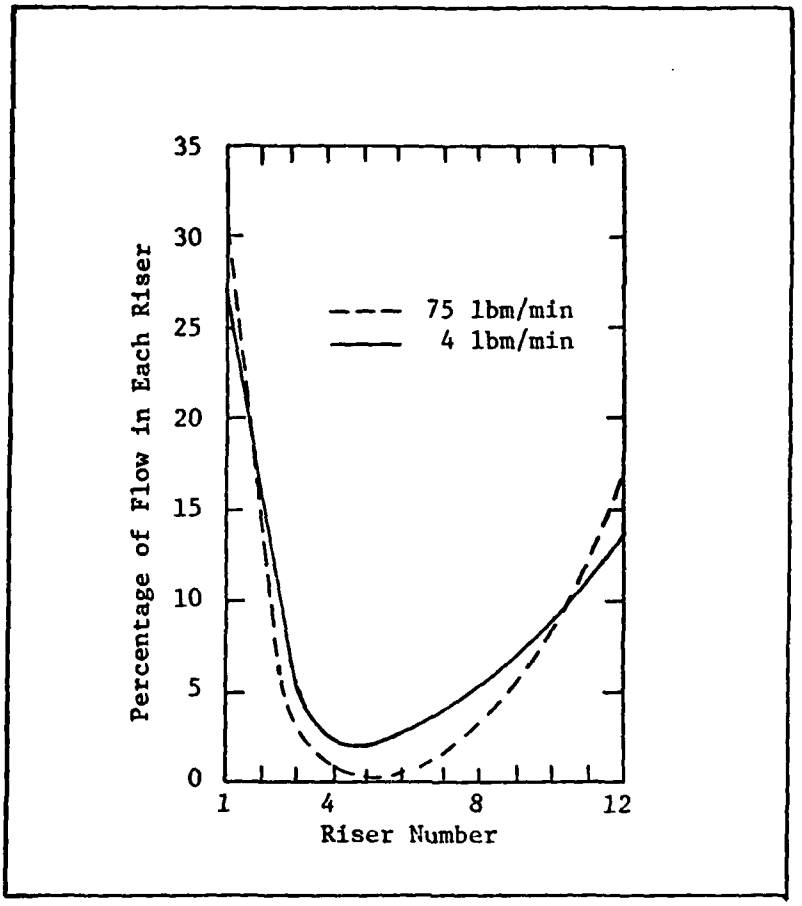

Figure 23 Flow Distribution with Increasing Flowrate

with the flow distribution shown in Figure 20 for all flowrates less than or equal to 4.44 lbm/min. Figure 23 shows changes resulting from pressure drop considerations alone when the total flowrate was increased.

Based on the summary of Metais and Eckert showing regions of mixed and free convection, and based on correlations with the flow model, it appears that free convection played a significant role in determining the flow distribution of the collector as used by the investigator.

This effect is not anticipated, however, for collectors in an operational environment since fluid would be entering at a relatively cooled condition and would be heated simultaneously and uniformly across the

absorber plate. Under this condition the aiding flow situation would probably tend to average out over the collector, resulting in a near uniform flow condition. However, since uniform distribution was easily disrupted by free convection effects or other unknown effects, it is concluded that the headers are undersized.

V Bond Conductance Test

The bond conductance is also a key parameter in the thermal performance of a solar collector, but like the internal heat transfer coefficient a point is ultimately reached where increasing values provide marginal to zero improvements in the collector efficiency factor. Whillier (Ref 15:95-98) studied the effect bond conductance has on the collector efficiency factor and showed that improvements beyond about 20 B/hr-ft-F are questionable.

The geometry of the tube-fin connection is of practical interest from the economical as well as thermal point of view. Whillier investigated two types of fin tube clamps shown in Figure 24. The wired fin consisted of a .02 inch thick copper fin wrapped three quarters of the way around a .83 inch diameter steel tube and pulled tight around the tube with thin galvanized steel wires at two inch spacings. The self clamping fin was constructed of .034 inch thick galvinized steel

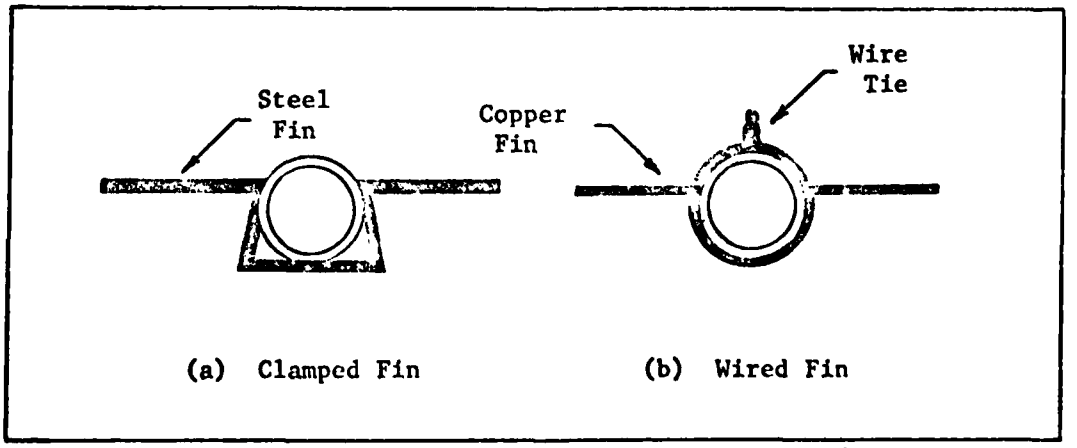

(Ref 16:95-98)

Figure 24 Fin Clamping Techniques Tested by Whillier

bent such that the tube could be spring loaded into the assembly as shown in Figure 24a.

The galvanized steel self clamping fin was tested twice-with and without soldering. It was significant that sometimes the soldered bond cracked immediately upon cooling due to thermal stresses. In fact, Whillier pointed out that it was hard to prevent the cracking. This points out one of the practical limitations of soldering.

The test showed that the self clamping fin had an average bond conductance of only 3.4 B/hr-ft-F. Soldering improved the results significantly, but Whillier was not able to obtain exact values from the test.

The wrapped and wired copper fin was superior with bond conductances being about 16 B/hr-ft-F. Whillier concluded that soldering was unnecessary provided the copper plate is wrapped aroung the tube and firmly clamped at two inch intervals.

Kahn (Ref 6:148-151) tested three other configurations for bond conductance. His apparatus consisted of three finned plates of galvanized steel each connected to a galvanized tube by one of the following:

(1) wired bond, C_b = 2.892 B/hr-ft-F
(2) soldered bond, C_b = 21.51 B/hr-ft-F
(3) Dupont Adhesive, C_b = 3.84 B/hr-ft-F.

Again it is seen that a soldered bond performs well, but it must be pointed out that conventional soldering techniques and continued thermal stresses encountered under operational conditions may render it impractical. The wired bond was well below the standards pointed out by Whillier, but Kahn only used six inch intervals for wiring where Whillier did so at two inch intervals. The .02 inch thick copper fin is also a very pliable material. Kahn did not specify the thickness of the fins

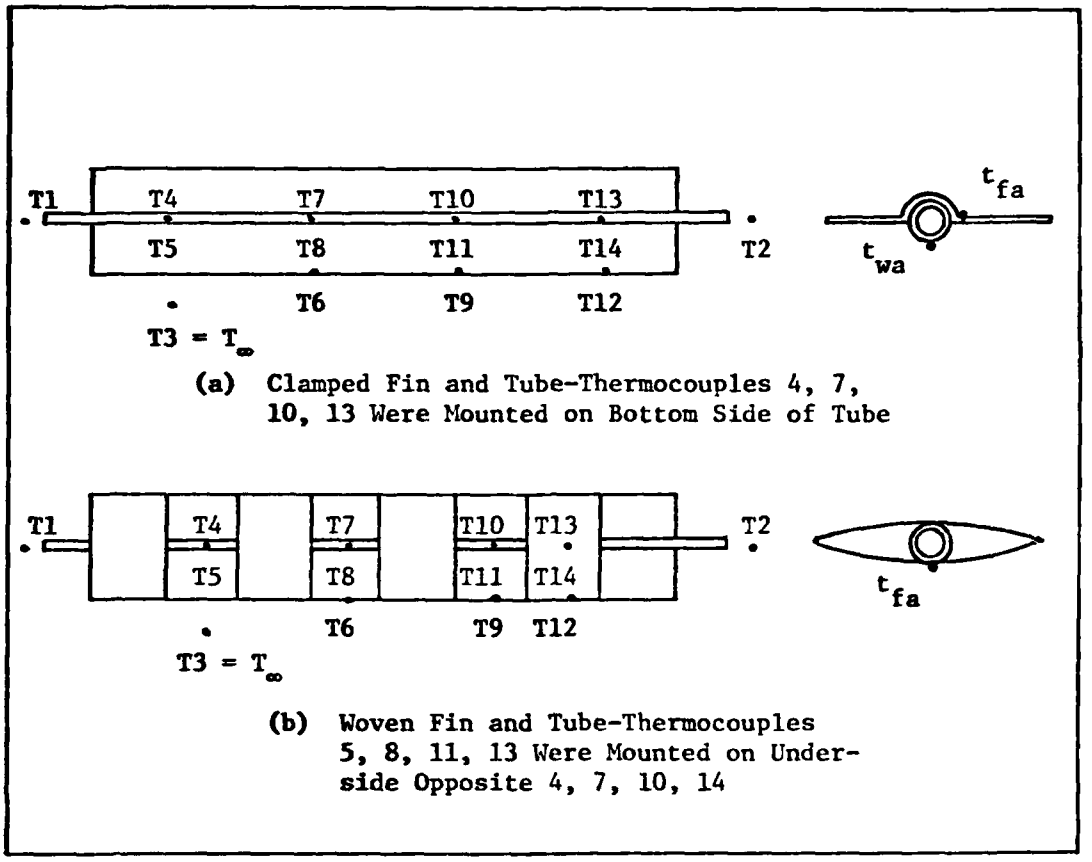

Figure 25 Schematic of the Bond Conductance Test Specimens and Thermocouple Locations

assessed in his paper, but unless it was thinner than .02 inch it certainly would be less pliable than the copper. Incidentally, since the thermal conductivity of copper is around one order of magnitude greater than galvanized steel, the thickness used by Kahn would have to be thicker than .02 inches to obtain comparable fin efficiencies with the copper fin. Thus, the number of wire ties, tightness of the clamp, pliability of the material, and construction detail all combine to define the bond conductance value and the difficulty or ease of fabrication.

Three more configurations were tested in this investigation. One was the clamped fin and tube; the other two were the woven fin and tube configuration shown in Figure 25 with and without thermal grease.

Test Description and Procedure

The apparatus for the test was the same as shown in Figure 8 except the test specimen was oriented horizontally. Like the internal heat transfer coefficient test, a single tube and fin was tested. Bond conductance was found by measuring the actual heat loss, the tube wall average temperature, and the average fin base temperature. The locations of the thermocouples are shown in Figure 25.

The bond conductance was computed according to:

$$C_b = \frac{WC_p(t_{fi} - t_{fo}) - Q_{loss}}{Y(t_{wa} - t_{fa})} \qquad (17)$$

where t_{wa} = average wall temperature
t_{fa} = average fin base temperature
Q_{loss} = energy lost directly from the tube to the atmosphere as defined in Appendix C

The heat loss term appearing in Eq (17) accounts for losses that do not occur through the bond. This energy passes directly from the exposed sections of the tube to the atmosphere and must be accounted for in the calculation.

Each configuration was tested at two flowrates to obtain an average value of bond conductance. In each case the system was allowed to run until equilibrium was reached. The mass flowrate and temperatures were recorded and the bond conductance computed. The woven fin configuration was tested with and without the thermal grease to assess its contribution to thermal performance.

Results

The experiment showed an average bond conductance for

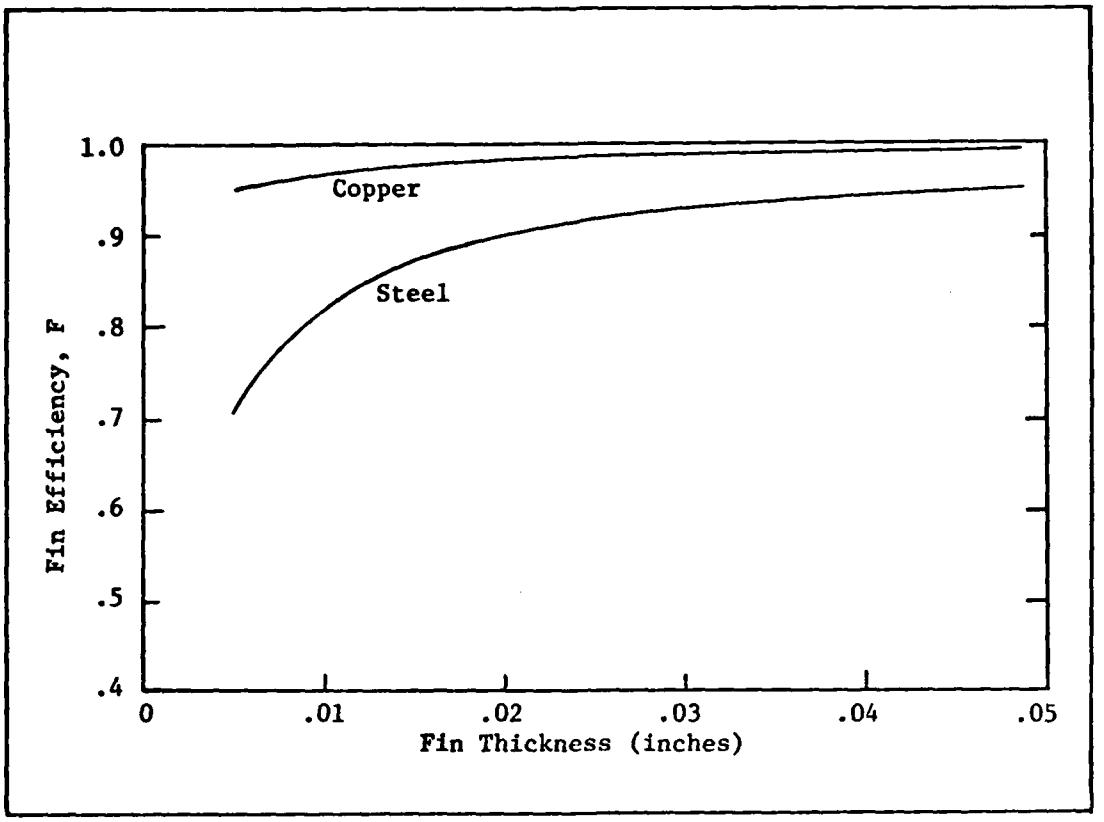

Figure 26 Fin Efficiency Versus Fin Thickness

a) clamped fin and tube, C_b = 18.88 B/hr-ft-F
b) woven fin and tube (no grease), C_b = 1.104 B/hr-ft-F
c) woven fin and tube (grease), C_b = 1.57 B/hr-ft-F.

Thus, the clamped fin and tube performed comparably with the wired clamping techniques reported by Whillier. But in his arrangement the tight bond was made possible by the thin, soft, and pliable copper sheet. The thicker steel used in this investigation was much too rigid to consider the wiring technique used by Whillier.

Since one strives for economy in collectors, steel fins make more sense to use. However, thicker steel is necessary to produce the comparable fin efficiencies obtained with copper, and it can be more difficult to install. Figure 26 makes the comparison. Using Eq (3)

for the fin efficiency, the length has been taken as four inches, U_L as .664 B/hr-ft^2-F, the conductivity of copper and steel as 220 and 26 B/hr-ft-F respectively. The comparison shows that steel thicknesses greater than .05 inches are required to compete thermally with .02 inch copper. Therefore, one has to choose some optimum thickness based on local material prices. And since increased steel thicknesses could result in degraded bond conductance, one has to consider this problem as well.

VI Long Wavelength Transmittance Test

During the last decade much attention has been given to finding a thermally suitable replacement for glass in solar collectors. This is due primarily to the weight, the ease with which it breaks, its high reflectivity unless treated, and it is hard to cut and handle. Fiberflass reinforced polyester resin materials such as Kalwall or other types of plastics on the other hand are very light-weight, hard to break, thermal shock resistant and easy to cut and handle. These advantages help minimize the maintenance and installation costs. Their main disadvantage, however, is transmittance in the far infrared range. Plastics also tend to deteriorate under ultraviolet radiation.

As the temperature of a blackbody increases, its emissive power also increases according to the spectral radiation distribution given by Planck's law (Ref 10:357-358):

$$e_{b\lambda} = \frac{2\pi C_1}{\lambda^5\left[\exp(C_2/\lambda T) - 1\right]} \tag{18}$$

where C_1 = first constant, .18892E8 B-μm^4/hr-ft^2

C_2 = second constant, 25898 μm-R

λ = wavelength μm

T = temperature R

$e_{b\lambda}$ = emissive power of a blackbody at wavelength λ, B/hr-ft^2-μm.

By using radiation tables it can be shown that about 93 percent of the sun's energy is radiated in the small wavelength region between zero and two micrometers. Thus to collect energy a collector's cover system must transmit in this range. The absorber plate temperature on the other

hand is characteristically less than 200 F and according to Eq (18) radiates most of its energy between two and forty micrometers. Therefore, in order to trap the energy received from the sun, the cover system should be opaque in this region.

Test Description and Results

This test was very simple to conduct. It was required to measure the long wavelength transmittance of the Kalwall cover. All that was necessary was the Kalwall cover, an isothermal flat plate with a known temperature, a thermopile, and potentiometer.

Heaters in the flat plate were adjusted to give a plate temperature of 154 F. The thermopile window was removed to increase sensitivity and the shutter opened to .3 centimeter.

The transmittance was measured by taking two readings with the potentiometer. One reading was made with the Kalwall between the plate and thermopile. The other reading was made without the Kalwall. The thermopile and flat plate remained stationary so that the ratio of the two potentiometer readings would give the transmittance of the cover. Care had to be taken not to leave the Kalwall in position too long because it would absorb radiation, increase in temperature, and cause the potentiometer reading to change. Thus, the reading had to be made rather quickly.

The test was actually conducted on .025 inch thick Kalwall and Visqueen material. The Visqueen was much thinner and more flimsy than the Kalwall but had about the same degree of opaqueness to visible light. The results of the test are presented in Table I.

A constant 154 F plate temperature was considered satisfactory

Table I Long Wavelength Transmittance Test Results of Kalwall and Visqueen

	Potentiometer Reading (mv)		
	With Cover	Without Cover	τ
Kalwall	2.	390.	.051
Visqueen	280.	390.	.717

because long wavelength transmittance characteristics do not vary much with temperature. Whillier (Ref 15:148-151) conducted a similar test for Tedlar plastic material and found that long wavelength transmittance properties varied only two percent under a temperature range of 0-200 C. Assuming Kalwall has similar characteristics (additional tests could easily be conducted to evaluate the long wavelength transmittance properties at various temperatures), the value reported in Table I is probably satisfactory for expected operational temperatures; and like glass, Kalwall is essentially opaque in the long wavelength region.

VII Overall Loss Coefficient-Heat Removal Factor Product Test

The instantaneous collector efficiency can be defined as the instantaneous useful energy gain, Eq (1), divided by the instantaneous energy available,

$$\eta = (\overline{\tau\alpha})F_R - U_L F_R(t_{fi} - t_\infty)/I \qquad (19)$$

The term, $(t_{fi} - t_\infty)/I$, is commonly used as the independent variable, so the $U_L F_R$ product is the slope of the efficiency curve. By measurement of the $U_L F_R$ product some insight is gained about the expected efficiency of the collector. The term, $(\overline{\tau\alpha})F_R$, is the "Y" intercept of the curve and represents the maximum attainable efficiency possible.

To obtain the best possible performance with the collector both the efficiency and the useful energy gain should remain high. A small overall loss coefficient and high heat removal factor ensures this criteria is met.

Both of these terms vary over the normal operating range though, so the slope can be expected to vary. Because of increasing losses with plate temperature the slope usually increases negatively and the efficiency begins to fall more rapidly as the mean plate temperature rises. But as discussed earlier and especially for this test where the operating temperatures were kept between 123-142 F this variation is very weak. Because of this fact a study of the heat removal factor as a function of the flowrate and collector configuration was permitted. Other variables such as the overall loss coefficient, collector efficiency, and collector area which make up the configuration were nearly constant and

served to define the maximum attainable value of the heat removal factor for each configuration.

Since hot water was pumped through the collector in lieu of irradiating it, the $U_L F_R$ product was simply computed by equating the useful energy gain with zero irradiation, Eq (1), to the measured enthalpy change of the water:

$$U_L F_R = \frac{WC_p(t_{fi} - t_{fo})}{A_c(t_{fi} - t_\infty)} \tag{20}$$

After the $U_L F_R$ product was measured it was possible to determine each term as well as fin efficiency, F, and the collector efficiency factor, F', separately. Two methods were used to reduce the data. One method used the expression for the mean plate temperature, i.e., Eq (11). From Eq (6) the other method found the product of $U_L F'$ given $U_L F_R$ and solved for the overall loss coefficient, U_L. Both methods were iterative.

The test was conducted on the following four configurations:

(1) Clamped fin with turbulators

(2) Clamped fin without turbulators

(3) Woven fin with turbulators

(4) Woven fin without turbulators.

Test Description and Procedure

The test set up was the same as that used in the flow distribution test for the fully assembled collector. A single thermocouple was attached midway and on the underside of each tube for all configurations. The readings from these twelve thermocouples were arithmetically averaged to compute an initial guess for the mean plate temperature. (This is

described in more detail later.) Mixed fluid temperatures were also recorded for the inlet and exit.

Results

A variety of information was extracted from this test. After measuring the $U_L F_R$ product for each operating condition, it was possible to compute the fin efficiency, collector efficiency factor, and the heat removal factor. These variables, the overall loss coefficient, and the mass flowrate have been summarized in Tables II and III for all four configurations. The heat removal factors have been shown as a function of flowrate and configuration in Figure 27. A single operating point from reference (5) has been included on Figure 27a for comparison.

The results using both reduction methods described earlier have been presented. Although confidence in one of the methods is not high, it is apparent that the clamped fin configuration is superior to the woven fin configuration. At the recommended flowrate of 3.3 lbm/min for instance, the clamped fin configuration had an approximate 13 percent improvement in the heat removal factor. Also shown in Figure 27a is the maximum possible value of F_R for this collector. This curve assumes infinite bond, internal heat transfer coefficient, and tube wall conductances. The difference between this curve and the curve generated without turbulators represents the improvement margin for the clamped fin configuration. The heat removal factor was computed with an overall loss coefficient of .664 B/hr-ft^2-F.

Figure 27a shows an approximate 2.5 percent improvement margin available for the collector without turbulators. When included the turbulators provide a nominal one percent additional improvement in the heat re-

TABLE II

Comparison of the $U_L F_R$ Test Results for the Clamped Fin and Tube Using Data Reduction Methods 1 and 2

Method 1

	Without Turbulators						With Turbulators	
W	.641	1.698	1.937	2.667	4.437	6.708	2.0	4.135
U_L	.525	.602	.578	.811	.926	1.317	.715	1.0
F	.952	.946	.948	.928	.919	.889	.936	.913
F'	.931	.921	.924	.897	.885	.844	.919	.896
F_R	.833	.878	.888	.862	.861	.824	.876	.868
$U_L F_R$	.437	.529	.513	.699	.797	1.085	.626	.872
t_{pm}	100	110	111	119	125	130	130	134
t_{fi}	123	136	131	136	132	132	135	137

Method 2

	Without Turbulators						With Turbulators	
W	.641	1.698	1.937	2.667	4.437	6.708	2.0	4.135
U_L	.632	.652	.646	.651	.648	.647	.653	.656
F	.943	.941	.942	.941	.942	.942	.941	.941
F'	.918	.916	.916	.916	.916	.916	.925	.929
F_R	.805	.869	.876	.886	.898	.904	.885	.909
$U_L F_R$	.509	.567	.566	.577	.582	.585	.578	.597
t_{pm}	116	131	127	130	128	127	131	134
t_{fi}	123	136	131	136	132	132	135	137

W - lbm/min t_{pm} - F

U_L - B/hr-ft^2-F t_{fi} - F

TABLE III

Comparison of the $U_L F_R$ Test Results for the Woven Fin and Tube Using Data Reduction Methods 1 and 2

Method 1

	Without Turbulators					With Turbulators		
W	1.687	2.75	4.28	7.45	9.0	1.5	2.56	5.96
U_L	.636	.681	.942	1.504	1.473	1.121	1.022	2.156
F	.937	.932	.909	.864	.866	.894	.903	.818
F'	.815	.804	.748	.652	.656	.723	.744	.587
F_R	.779	.781	.73	.639	.646	.668	.712	.569
$U_L F_R$	.495	.532	.688	.961	.951	.749	.728	1.227
t_{pm}	121	121	128	135	134	129	131	135
t_{fi}	141	142	140	140	138	134	135	138

Method 2

	Without Turbulators					With Turbulators		
W	1.687	2.75	4.28	7.45	9.0	1.5	2.56	5.96
U_L	.651	.652	.647	.640	.639	.634	.638	.632
F	.935	.935	.935	.936	.936	.937	.936	.937
F'	.811	.811	.812	.814	.814	.823	.823	.828
F_R	.775	.788	.797	.805	.807	.781	.798	.817
$U_L F_R$	.504	.514	.516	.515	.515	.495	.509	.516
t_{pm}	130	130	127	122	121	118	121	117
t_{fi}	141	142	140	140	138	134	135	138

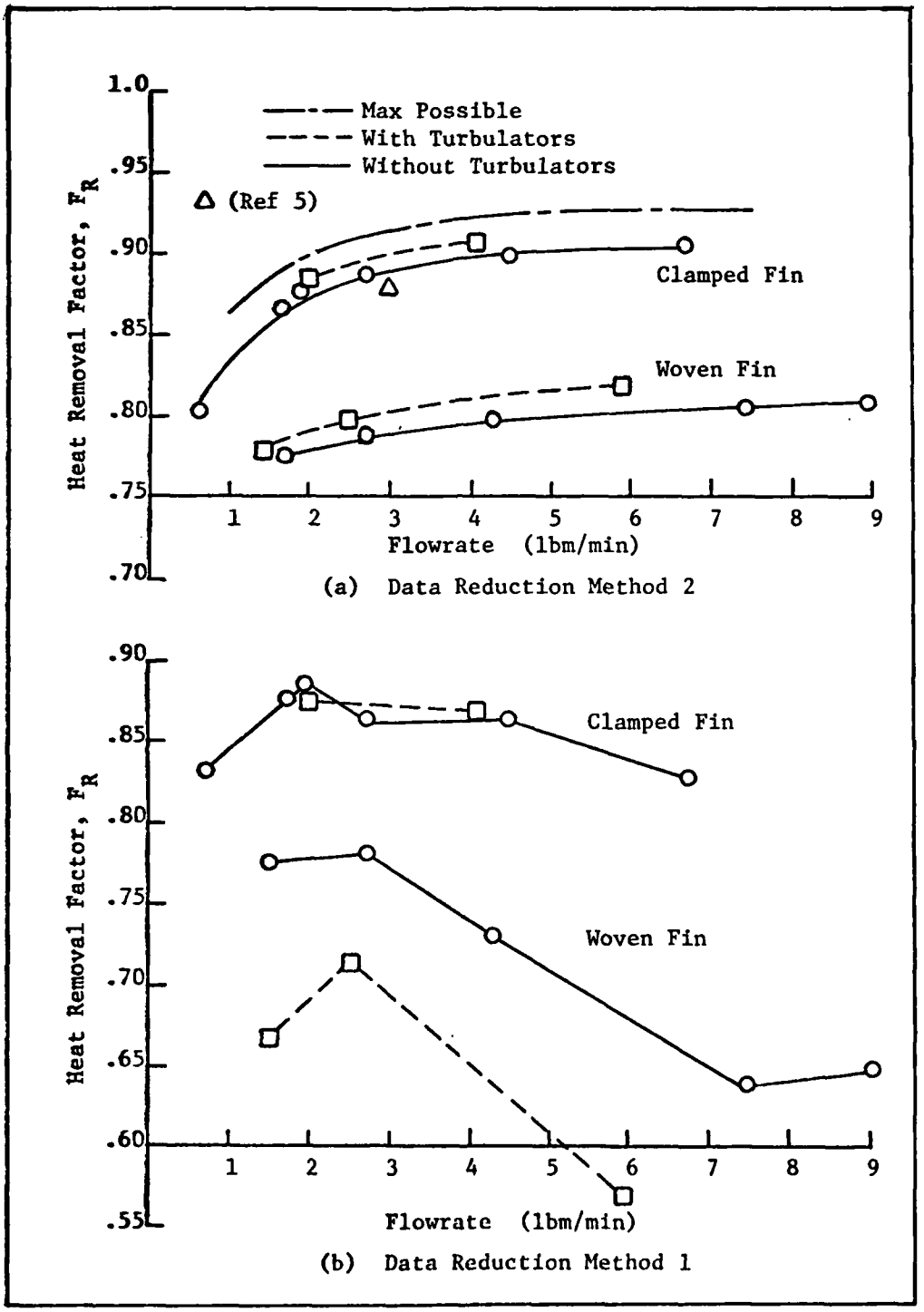

Figure 27 Heat Removal Factor Versus Flowrate

moval factor. Section III alluded to this marginal return when the effect of the internal heat transfer coefficient and bond conductance on the collector efficiency factor was demonstrated. Recall that improvements in these variables above 50 B/hr-ft^2-F and 20 B/hr-ft-F respectively effected minimal improvement on the collector efficiency factor. Figure 27a shows there is little impact on the collector heat removal factor as well.

Discussion

As pointed out earlier two methods were used to compute the fin efficiency, collector efficiency factor, heat removal factor, and the overall loss coefficient for each operating condition where the $U_L F_R$ product was measured. For reasons pointed out later, the results of the first method were not good. The heat removal factor calculated by this method is shown in Figure 27b. Other variables are listed in Tables II and III.

The method for reducing the data was very simple. First, Eq (6) was solved for the product of the overall loss coefficient and collector efficiency factor:

$$U_L F' = -\frac{WC_p}{A_c} \text{Log}_e\left[1 - U_L F_R A_c / WC_p\right] \qquad (21)$$

The term on the right hand side of Eq (21) was set equal to a constant depending on the measured quantities. Having determined the internal heat transfer coefficient and bond conductance from previous tests, the overall loss coefficient was computed by expressing the collector efficiency factor in terms of the overall loss coefficient and solving Eq (21) iteratively. Afterwards, the fin efficiency, collector effi-

iciency factor, and heat removal factors were found from Eq (2), (21), and (6) respectively.

The second method was equally simple. First, it was assumed that the predicted overall loss coefficient as shown in Appendix D (Figure D-1) was correct. Assuming a plate temperature-the first guess being the arithmetic average of the twelve thermocouple readings-an overall loss coefficient was computed. Then as in the first method the fin efficiency, collector efficiency factor, and the heat removal factors were computed. Using Eq (11) and the measured energy exchange, Q_u, a mean plate temperature was computed. The process was repeated until no change in the mean plate temperature occurred. Sample calculations are provided in Appendix D.

A comparison of Figures 27a and b shows a significant difference in the results of the methods. A likely explanation comes from unsteady conditions which were present throughout the test. The inability to obtain a truly steady state condition was evident from the onset of the experiment and was the reason for including the submersible heater and insulation around the flexible hose. The problems obtaining steady state conditions are summarized in Figure 28 for two flowrates which are about the same (4.135 lbm/min versus 4.5 lbm/min). The results are shown with and without the submersible heater and insulation. Data was taken over a 4.8 hour period without the heater. The $U_L F_R$ product was seen to vary from .684 - .972 B/hr-ft^2-F (a 42 percent variation). When the heater and insulation were added the variation was reduced to 12 percent with values of the $U_L F_R$ product varying between .816 - .915 B/hr-ft^2-F. The figure shows that the collector temperature difference, $(t_{fi} - t_{fo})$, was a little more uniform during the test with the heater; however, a signif-

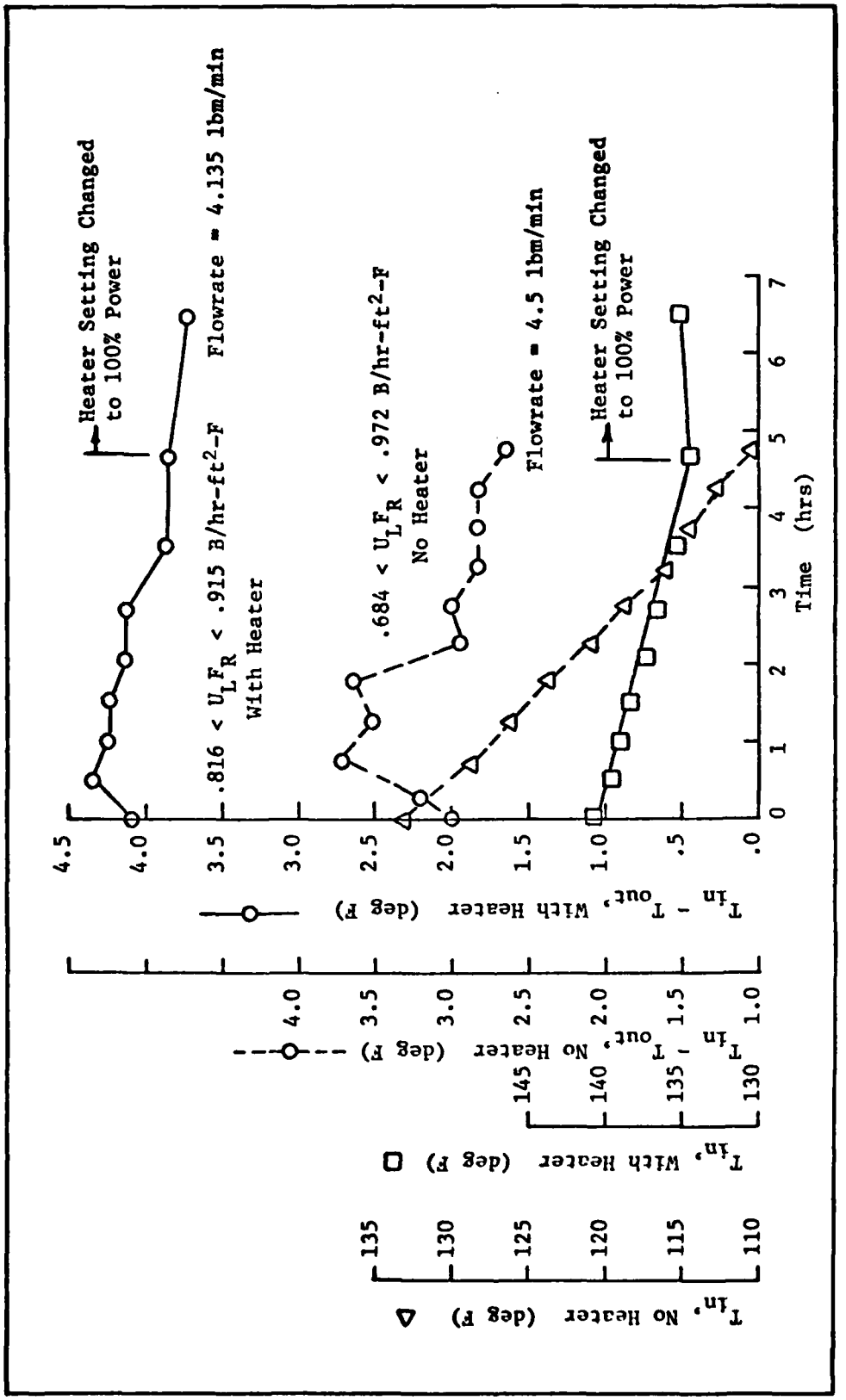

Figure 28 Data Illustrating the Unsteady Condition Present During the $U_L F_R$ Product Test

icant temperature difference decrease was still prevalent.

Also plotted on Figure 28 is the collector inlet temperature versus time. Again, the heater and insulation addition significantly reduce the slope, but it is evident that steady state was still not achieved-even after more than four hours of operation at constant mass flowrate.

Small increases in the recorded ambient temperature were also noted throughout the test. For instance, the ambient temperature increased from 66 F to 68.5 F over the 4.8 hour period for the run without the heater. This increase was typical throughout the test. However, everything else being constant, this variation resulted in only a 3.8 percent change in the $U_L F_R$ product. Therefore, changes in the ambient temperature do not account for the large variations in the $U_L F_R$ product reported in Tables II and III. Likewise, since the flowrate was constant and the laboratory provided a no wind condition, the most likely explanation for the varying overall loss coefficient as computed by the first method stems from unsteady effects.

To explain the effect assume for the moment that the inlet and ambient temperatures remain fixed and the flowrate is allowed to increase. It can be deduced that the mean plate temperature will rise at a rate prescribed by the actual heat transfer characteristics and the thermal capacitance of the collector. Because of the thermal capacitance the actual mean plate temperature lags the steady state value. Consequently, the outlet temperature also lags the steady state value and results in higher $U_L F_R$ values according to Eq (20).

Since more heat transfer occurs at higher flowrates more time is required to achieve steady state conditions, and recording data consistently too early (this was done at approximately two hour intervals) after

each flowrate change would result in progressively larger errors for each point. This is precisely the effect shown in Tables II and III where increasing values of the overall loss coefficient and the $U_L F_R$ product are noted for method 1.

The result using method 2 better illustrates the expected outcome of the test, but for two reasons is nothing more than a theoretical prediction of the heat removal factor with flowrate. The first and foremost reason is that a predicted value of the overall loss coefficient was used. Second, even though the measured enthalpy change was used in the calculations and reduced the mean plate temperature below that of the fluid inlet, the change in the overall loss coefficient was negligible from one iteration to the next. Therefore, the results presented in Figure 27a behave as a theoretical prediction based on the overall loss coefficient calculation and as such contribute little to this experimental investigation. However, the information shown is not without merit.

Work on this collector conducted by Groves (Ref 5) established the overall loss coefficient from which Figure D-1 was derived. Furthermore, work completed under this investigation defined the internal heat transfer coefficient and bond conductance for each of the other configuations as well. So, Figure 27a is, after all, a complete and accurate assessment of the heat removal factor for all four of the tested configurations.

VIII Summary

This investigation dealt with several parameters defining the thermal performance characteristics of a liquid heating-flat plate solar collector. These were:

(1) Internal heat transfer coefficient
(2) Flow distribution
(3) Bond Conductance
(4) Long Wavelength transmittance characteristics
(5) $U_L F_R$ product

Two types of absorber plates-clamped and woven fins-were tested for bond conductance characteristics. The effects of turbulators on the internal heat transfer coefficient were also examined.

Internal Heat Transfer Coefficient

The mean Nusselt number varied between 6.68 and 7.7 for the tube without turbulators. This corresponds to internal heat transfer coefficient values between 98-114 B/hr-ft^2-F for water at 150 F.

Mean values were much higher with turbulators. They ranged from 9.76-20.07 for flowrates between 4.86-20.45 lbm/hr/tube. This resulted in heat transfer coefficients between 254-522 B/hr-ft^2-F.

Only an approximate one percent improvement in the heat removal factor was obtained when turbulators were included. So it was concluded that turbulators did not significantly improve overall performance.

Flow Distribution

The use of turbulators helps ensure a more uniform flow distribution for this collector. With the turbulators removed and with hot water pumped through the collector a greater portion of the flow was apparently

passing through the first risers. As the flowrate was increased flow in each successive riser starting with the inlet, also increased. Only under the highest flowrate of 6.7 lbm/min did the flow appear to be uniform.

Since the tubes will be heated uniformly under solar irradiation-assuming no blockage of tubes-the flow distribution will probably be adequate even without turbulators. However, with the small 3/4 inch diameter headers, it was shown that a maladjusted flow pattern was easily achieved. Therefore, in order to reduce the risk of unbalanced flow, it was concluded that header diameters should be increased.

Bond Conductance

The clamped fin configuration resulted in an average test value of 18.88 B/hr-ft-F. This value was considered satisfactory since it was shown that higher values resulted in marginal thermal performance returns.

The woven fin was unacceptable. The average test value result was 1.104 B/hr-ft-F. With a generous application of Insulgrease this value was improved to 1.57 B/hr-ft-F.

Long Wavelength Transmittance Characteristics

The Kalwall material which was .025 inches thick was essentially opaque to far infrared radiation. The measured value was 5.1 percent which was considered excellent.

$U_L F_R$ Product

The test results were inconclusive since steady state operating conditions were never achieved. However, based on a predicted value of the overall loss coefficient which compared quite closely to an

experimentally determined value from previous work (Ref 5), a summary study of the heat removal factor as a function of flowrate was made. This summary compared the clamped and woven fin configurations and also included the effects of turbulators.

The results of the summary showed the clamped fin configuration performed 13 percent better than the woven fin configuration. The use of turbulators only increased the heat removal factor by a nominal one percent.

IX Conclusions

From the results of this investigation the following conclusions are drawn:

(1) The use of turbulators greatly enhanced the internal heat transfer coefficient, but unfortunately, made little difference in the overall performance.

(2) The use of turbulators improved flow uniformity by increasing the pressure drop in the tubes.

(3) The diameter of the headers should be larger to help ensure flow uniformity. This is especially true for low flowrate conditions such as those tested.

(4) The bond conductance for the clamped fin was competitive with soldering since little gain in performance is realized after a value of 20 B/hr-ft-F is achieved.

(5) The bond conductance of the woven fin configuration was unacceptable, AND

(6) Kalwall material was essentially opaque to far infrared radiation.

Bibliography

1. Baker, L. H., "Film Heat Transfer Coefficients in Solar Collector Tubes at Low Reynolds Numbers," Solar Energy, vol. 11, no. 2, 1967, pp. 78-85.

2. Beckman, W. A., and Duffie, J. A., Solar Energy Thermal Processes, New York, John Wiley and Sons, 1974, pp. 108-177.

3. Brown, A. R., and Thomas, M. A., "Combined Free and Forced Convection Heat Transfer for Laminar Flow in Horizontal Tubes," Journal of Mechanical Engineering Science, vol. 7, no. 4, 1965, pp. 440-448.

4. Dunkle, R. V., and Davey, E. T., "Flow Distribution in Absorber Banks," Paper presented at Melboutne International Solar Energy Society Conference (1970).

5. Groves, C. E., "Investigation of the Thermal Performance of a Low Cost Liquid-Heating Flat Plate Solar Collector Using a Solar Simulator," Thesis, The Air Force Institute of Technology, 1977.

6. Kahn, Ehsan Ullah, "Evaluation of Bond Conductance in Various Tube-in-Strip Types of Solar Collectors," Solar Energy, vol. 7, no. 3, 1963, pp. 148-151.

7. Kays, W. M., Convective Mass and Heat Transfer, New York, McGraw Hill, 1966, pp. 102-144.

8. Kemeny, G. A., and Somers, E. V., "Combined Free and Forced-Convective Flow in Vertical Circular Tubes-Experiments with Water and Oil," Journal of Heat Transfer, vol. 84, 1962, pp. 339-346.

9. Klien, S. A., "The Effects of Thermal Capacitance Upon the Performance of Flat Plate Solar Collectors," Thesis, University of Wisconsin, 1973.

10. Kreith, F., Principles of Heat Transfer, Scranton, Pennsylvania, International Text Book, 1965, pp. 357-358.

11. McComas, S. T., and Eckert, E. R. G., "Combined Free and Forced Convection in a Horizontal Circular Tube," Transactions ASME, Journal of Heat Transfer, vol. 88, series C, 1966, pp. 147-153.

12. Metais, B., and Eckert, E. R. G., "Forced, Mixed, and Free Convection Regimes," Journal of Heat Transfer, vol. 86, 1964, pp. 295-297.

13. Oliver, D. R., "The Effect of Natural Convection on Viscous-Flow Heat Transfer in Horizontal Tubes," Chemical Engineering Science, vol. 17, 1962, pp. 335-350.

14. SAE Aerospace Applied Thermodynamics Manual, SAE Committee AC-9, Aircraft Environmental System, Society of Automotive Engineers, Inc., New York, New York, p. 83.

15. Whillier, A., "Plastic Covers for Solar Collectors," Solar Energy, vol. 7, no. 3, 1963, pp. 148-151.

16. Whillier, A., "Thermal Resistance of the Tube-Plate Bond in Solar Heat Collectors," Solar Energy, vol. 8, no. 3, 1964, pp. 95-98.

Appendix A

Internal Heat Transfer Coefficient

Included in this appendix are the derivation of Eq (12) and (13), water property assumptions, sample calculations, data, and results.

Derivations

A description of the local bulk temperature along the tube is necessary to compute the local Nusselt number. The temperature change was assumed to be an exponential function, and it was further assumed that the fin loss coefficient was constant.

Writing an energy balance for a differential element results in

$$WC_p \frac{dt_f}{dx} = h_x \pi D_h (t_w - t_f) = UL(t_\infty - t_f) \qquad \text{(A-1)}$$

where x has been taken as the tube direction, t_w is the local wall temperature, L is the width of the fin, t_f is the local bulk temperature, and U is a constant fin loss coefficient. The boundary condition is

$$t_f = t_{fi} \text{ at } x = 0$$

The solution of this is Eq (12) where

$$\frac{UL}{WC_p} = \frac{-\text{Log}_e}{Y}\left[\frac{t_{fo} - t_\infty}{t_{fi} - t_\infty}\right] \qquad \text{(A-2)}$$

for Y equal to the tube length. The local Nusselt number is simply defined by equating the last two terms of Eq (A-1) and solving for the local heat transfer coefficient.

Property Assumptions

The viscosity, Prandtl number, and thermal conductivity were assumed to vary with temperature alone according to

$$\mu\left[\frac{\text{lbm}}{\text{hr-ft}}\right] = (7.85077\text{E-}5)T^2 - (3.37417\text{E-}2)T + 4.346 \qquad \text{(A-3)}$$

$$Pr = (2.0575\text{E-}4)T^2 - (8.9214\text{E-}2)T + 11.4927 \qquad \text{(A-4)}$$

$$k\left[\frac{B}{\text{hr-ft-F}}\right] = a_1T_R^4 + a_2T_R^3 + a_3T_R^2 + a_4T_R + a_5 \qquad \text{(A-5)}$$

where $a_1 = -3.8228\text{E-}12$

$a_2 = 1.2059\text{E-}8$

$a_3 = -1.5038\text{E-}5$

$a_4 = 8.6283\text{E-}3$

$a_5 = -1.495$

T = degrees F

T_R = degrees R

In the calculation of the Grashof number

$$\beta\left[\frac{1}{F}\right] = -\frac{B + 2CT}{A + BT + CT^2} \qquad T \text{ in degrees F} \qquad \text{(A-6)}$$

$$\rho\left[\frac{\text{lbm}}{\text{ft}^3}\right] = a_1T^4 + a_2T^3 + a_3T^2 + a_4T + a_5 \qquad \text{(A-7)}$$

where $a_1 = -1.8182\text{E-}10$

$a_2 = 5.425\text{E-}7$

$a_3 = -6.4108\text{E-}4$

$a_4 = 3.2185\text{E-}1$

$a_5 = 5.2289$

$A = 62.5375$

$B = 1.6521\text{E-}3$

C = -7.093E-5

T = arithmetically averaged bulk temperature in degrees R except as noted

Sample Calculations

The inside diameter of the tube was measured at 5/16 inch. The turbulator dimensions were taken as .025 inch thick with the width equal to the inside diameter of the tube. This resulted in hydraulic diameters of .02604 and .014755 feet without and with turbulators respectively.

The local wall temperature was measured at eight equally spaced stations along the tube. The inlet and outlet temperatures were fluid bulk temperatures.

This sample calculation compiles the local Nusselt number at station 2 for the first set of data (see Data and Results this Appendix). Following that is a calculation of the mean Nusselt number:

Station	Bulk Fluid Temperature	Wall Temperature (least squares)
1	159.39 F	
2	152.79	144.93 F
3	140.95	132.37
4	130.73	122.51
5	121.9	114.81
6	114.27	108.73
7	107.69	103.73
8	102.0	99.27
9	97.09	94.79
10	94.89	

where ambient temperature = 66 F

flowrate = 4.8601 lbm/hr

hydraulic diameter = .014755 ft

Reynolds number = $86.292 \frac{W}{\mu}$

$$\frac{UL}{WC_P} = \frac{-\log_e\left[\frac{94.89 - 66}{159.39 - 66}\right]}{4}$$

$$= .2933 \text{ ft}^{-1}$$

$$t = (159.39 - 66)\exp(-.2933x) + 66$$

$x = 3/12$ feet for station 2

$x = 9/12$ feet for station 3, etc.

$t = 152.79$ F

$$k = a_1(612.79)^4 + a_2(612.79)^3 + a_3(612.79)^2 + a_4(612.79)^1 - 1.495$$

$$= .3812 \text{ B/hr-ft-F}$$

$$\frac{UL}{k\pi} = \frac{.2933(4.8601)(1)}{(\pi)(.3812)} = 1.1903$$

$$Nu_x = \frac{1.1903(159.39 - 66)\exp(-.2933x)}{(159.39 - 66)\exp(-.2933x) + 66 - 144.93}$$

$$Nu_x = 13.15$$

The experimental mean Nusselt number is calculated as follows:

$$Nu_m = \frac{h_m D_h}{k} \qquad \text{(A-8)}$$

where

$$h_m = \frac{UL(t_\infty - t_{f\ avg})}{\pi D_h (t_{wall\ avg} - t_{f\ avg})} \qquad \text{(A-9)}$$

For the data shown $t_{f\ avg} = 122.17$

$t_{wall\ avg} = 115.14$

$k_{avg} = .3717$

$$Nu_m = 1.2207 \frac{(66 - 122.17)}{(115.14 - 122.17)}$$

$$Nu_m = 9.75$$

The above average properties were used when correlating data with Thomas' and Oliver's equations. In addition, the Graetz number was defined as

$$Gz = WC_p/kY$$

where Y is the length of the tube. The tube hydraulic diameter was used in the Grashof number.

Data and Results

This section contains a listing of the results. The first four pages are data for tubes with turbulators. The remaining four data pages are without turbulators. The wall temperatures are predicted using a least squares curve fit of the recorded temperature data shown above the results on each page. Appearing just below the station results is the average viscosity based on the average bulk and wall temperatures respectively. Average values of Reynolds and Prandtl numbers as well as average wall and bulk temperatures are given. Finally, mean values according to Oliver's, Thomas', and experimental results are shown.

1 WDOT = 4.8601 (MASS FLOWRATE---LBM/HR)

TEMPERATURES ARE: T1 THRU T10---DEGREES F
159.3900 144.9400 132.4300 122.3700 114.7600
108.9500 103.7900 99.0200 94.8900 94.8900

STA	TWALL	X/DH	REX	PRX	INVGZX2	TBULK	NUX(LOG)
1	*********	0.000	*********	******	****	159.390	******
2	144.934	16.940	409.810	2.6649	.031	152.788	13.153
3	132.369	50.820	764.737	3.0057	.093	140.948	10.491
4	122.512	84.710	328.487	3.3462	.154	130.726	9.544
5	114.813	118.600	299.660	3.6750	.215	121.896	9.638
6	108.734	152.490	274.740	3.9848	.277	114.270	10.732
7	103.732	186.380	258.417	4.2716	.338	107.635	13.075
8	99.266	220.260	249.867	4.5335	.399	102.000	16.434
9	94.789	254.150	231.693	4.7725	.460	97.088	16.977
10	*********	271.090	*********	******	****	94.890	******

AMUB= 1.396 AMUB= 1.502 RAVG=301.652
PRAVG= 3.782 TWAVG=115.144 TBAVG=122.168
MEAN CRASHFF= .4645145+04 GRATZ = 3.269

OLIVERS CORRELATION---> NUMO= 4.359
THOMAS CORRELATION----> NUMT= 3.103
EXPERIMENTAL DATA-----> NUX = 9.763

1 WDOT = 7.5930 (MASS FLOWRATE---LBM/HR)

TEMPERATURES ARE: T1 THRU T10---DEGREES F
131.0100 125.7210 122.7500 119.9200 117.2100
114.9900 112.3100 110.1100 108.3100 109.0400

STA	TWALL	X/DH	REX	PRX	INVG/X2	TBULK	NUX(LOG)
1	*********	0.000	********	******	****	131.010	******
2	125.700	16.940	[illegible]	3.3959	.020	129.335	11.739
3	122.771	50.830	489.245	3.5137	.059	126.122	12.084
4	119.950	84.710	473.997	3.6290	.098	123.083	12.259
5	117.258	118.600	459.089	3.7416	.138	120.208	12.351
6	114.720	152.490	447.116	3.8512	.177	117.488	12.481
7	112.359	186.380	435.278	3.9576	.216	114.916	12.813
8	110.199	220.260	424.393	4.0608	.256	112.484	13.598
9	108.263	254.150	414.342	4.1607	.295	110.193	15.342
10	*********	271.090	*********	******	****	109.080	******

RHOB= 1.437 AMUB= 1.482 RAVG=456.276
PRVG= 3.789 TWAVG=116.403 TBAVG=119.391
MEAN CRASHOF= .181947E+04 GRAIZ = 5.121

OLIVERS CORRELATION---> NUM= 3.921
THOMAS CORRELATION----> NUM= 3.499
EXPERIMENTAL DATA-----> NUM = 12.001

1 WDOT = 14.2810 (MASS FLOWRATE---LBM/HR)

TEMPERATURES ARE: T1 THRU T10---DEGREES F

144.9400 139.7800 138.1100 136.1700 134.1100
132.0400 130.2400 128.4300 126.6200 128.4300

STA	TWALL	X/DH	REX	PRX	INVGZX2	TBULK	NUX(LOG)
1	*********	0.000	**********	******	****	144.940	******
2	139.821	16.940	1102.719	2.9188	.011	143.784	13.903
3	138.044	50.830	1077.991	2.9878	.032	141.524	15.378
4	136.133	84.710	1054.372	3.0566	.053	139.333	16.236
5	134.147	118.600	1031.815	3.1252	.074	137.210	16.475
6	132.147	152.490	1010.292	3.1935	.095	135.151	16.309
7	130.193	186.380	989.762	3.2614	.115	133.155	16.060
8	128.347	220.260	970.193	3.3287	.136	131.221	16.070
9	126.668	254.150	951.529	3.3955	.157	129.346	16.747
10	*********	271.090	**********	******	****	128.430	******

AMUB= 1.264 AMUW= 1.245 AVC=*******
PRAVG= 3.154 TWAVG=133.188 TBAVG=136.409
MEAN GRASHOF= .3217068+04 GRATZ = 9.483

OLIVERS CORRELATION----> NUMO= 4.555
THOMAS CORRELATION-----> NUMT= 4.582
EXPERIMENTAL DATA------> NUM = 15.483

1 WDOT = 20.4530 (MASS FLOWRATE---LBM/HR)

TEMPERATURES ARE: T1 THRU T10---DEGREES F
151.2600 146.8700 145.9700 144.6800 142.8900
141.2000 140.3000 138.8800 137.4600 138.8800

STA	TWALL	X/DH	REX	PRX	INVGZX2	TBULK	NUX(LOG)
1	********	0.000	********	******	****	151.260	******
2	146.970	16.940	1695.927	2.7284	.007	150.424	16.475
3	145.837	50.830	1659.181	2.7739	.022	148.778	18.969
4	144.500	84.710	1623.182	2.8195	.037	147.167	20.515
5	143.040	118.600	1587.914	2.8653	.051	145.588	21.045
6	141.536	152.490	1553.377	2.9111	.066	144.042	20.982
7	140.070	186.380	1519.562	2.9569	.081	142.528	20.972
8	138.723	220.260	1486.465	3.0026	.095	141.046	21.749
9	137.573	254.150	1454.060	3.0483	.110	139.595	24.508
10	********	271.090	********	******	****	138.880	******

AMUB= 1.105 AMUW= 1.134 RAVG=*******
PAVG= 2.888 TWAVG=142.281 TBAVG=144.931
MEAN GRASHOF= .334829E+04 GRATZ = 13.489

OLIVERS CORRELATION---> NUMO= 4.854
THOMAS CORRELATION----> NUMT= 5.275
EXPERIMENTAL DATA-----> NUM = 20.071

WCCT = 4.6450 (MASS FLOWRATE---LBM/HR)

TEMPERATURES ARE: T1 THRU T10---DEGREES F

148.8100	138.3600	133.5900	128.6900	123.7900
119.4000	116.0500	112.9500	109.5960	111.4020

STA	T-ALL	X/DH	REX	PRX	INVGRX2	TBULK	NUX(LOG)
1	*********	0.000	*********	******	****	148.810	******
2	138.494	9.599	207.020	2.8635	.032	145.647	6.749
3	133.391	28.800	195.057	3.0445	.097	139.713	7.041
4	129.522	48.000	184.502	3.2234	.161	134.268	7.142
5	123.949	67.200	175.217	3.3982	.226	129.270	7.109
6	119.733	86.410	167.052	3.5679	.290	124.681	7.046
7	115.941	105.610	159.877	3.7311	.354	120.472	7.091
8	112.635	124.800	153.562	3.8872	.418	116.611	7.446
9	109.760	144.000	147.743	4.0427	.485	112.907	8.634
10	*********	153.210	*********	******	****	111.402	******

AMLP= 1.305 AMUW= 1.386 RAVG=173.754
PAVG= 3.470 TWAVG=122.803 TRAVG=128.378
MEAN GRASHOF= .243150E+08 GRATZ = 3.106

CLIVERS CORRELATION---> NUVC= 6.137
THOMAS CORRELATION----> NUVT= 3.464
EXPERIMENTAL DATA-----> NUV = 6.682

WCCT = 8.8860 (MASS FLOWRATE---LBM/HR)

TEMPERATURES ARE: T1 THRU T10---DEGREES F
147.9100 138.1050 135.5250 132.4290 129.2040
125.8500 123.9150 121.4640 119.0130 122.7540

STA	TWALL	X/DM	RFX	PRX	INVGZX2	TBULK	NUX(LOG)
1	*********	0.000	*********	******	****	147.910	******
2	138.241	9.599	357.577	2.8521	.017	146.040	7.068
3	135.317	28.800	383.522	2.9599	.051	142.430	7.407
4	132.293	48.000	370.419	3.0076	.084	138.990	7.519
5	129.270	67.200	358.225	3.1748	.118	135.711	7.473
6	126.350	86.410	346.886	3.2811	.152	132.584	7.379
7	123.638	105.610	336.359	3.3862	.185	129.605	7.366
8	121.235	124.800	326.590	3.4897	.219	126.767	7.594
9	119.160	144.900	317.105	3.5962	.254	123.937	8.386
10	*********	153.210	*********	******	****	122.754	******

AMLP= 1.226 AMUM= 1.311 RAVG=354.586
PAVG= 3.226 TWAVG=128.189 TBAVG=134.673
MEAN GRASHOF= .338855E+05 GRATZ = 5.909

CLIVERS CORRELATION---> NUMC= 6.625
THOMAS CORRELATION-----> NUMT= 4.636
EXPERIMENTAL DATA-----> NUM = 7.313

WCCT = 14.6120 (MASS FLOWRATE---LBM/HR)

TEMPERATURES ARE: T1 THRU T10---DEGREES F
129.4920 131.9130 129.5910 128.0430 126.1090
124.1730 123.0120 121.7220 120.1740 124.4310

STA	TWALL	Y/DH	REX	PPX	INVCZX2	TBULK	NUX(LOG)
1	*********	0.000	*********	******	****	138.492	******
2	131.883	9.599	600.035	3.1152	.010	137.515	8.499
3	129.753	28.800	588.415	3.1784	.031	135.604	7.963
4	127.818	48.000	577.291	3.2411	.051	133.747	7.648
5	126.056	67.200	566.644	3.3035	.072	131.942	7.497
6	124.444	86.410	556.451	3.3654	.092	130.187	7.477
7	122.961	105.610	546.703	3.4267	.113	128.483	7.568
8	121.596	124.800	537.381	3.4874	.133	126.828	7.758
9	120.335	144.900	528.047	3.5503	.155	125.145	8.052
10	*********	153.210	*********	******	****	124.431	******

AMLP= 1.270 AMUW= 1.347 RAVG=562.621
PAVG= 3.334 TWAVG=125.592 TBAVG=131.237
MEAN GRASHOF= .267429E+05 GRATZ = 9.746

CLIVERS CORRELATION----> NUSS= 6.562
THOMAS CORRELATION-----> NUST= 5.564
EXPERIMENTAL DATA------> NU* = 7.732

WCCT = 20.9410 (MASS FLOWRATE---LBM/HR)

TEMPERATURES ARE: T1 THRU T10---DEGREES F
138.6210 133.3300 130.3650 129.3300 128.0400
126.4950 126.2370 124.8200 124.1700 129.0800

STA	TWALL	X/DH	REX	PRX	INVGZX2	TBULK	NUX(LOG)
1	*********	0.000	*********	******	****	138.621	******
2	133.153	9.599	864.033	3.1001	.007	137.982	9.315
3	130.828	28.800	852.987	3.1413	.021	136.722	7.499
4	129.092	48.000	842.250	3.1823	.036	135.485	6.792
5	127.797	67.200	831.813	3.2233	.050	134.271	6.591
6	126.795	86.410	821.665	3.2640	.064	133.079	6.674
7	125.950	105.610	811.809	3.3046	.079	131.909	6.910
8	125.105	124.800	802.235	3.3449	.093	130.762	7.151
9	124.064	144.000	792.499	3.3870	.108	129.584	7.196
10	*********	153.210	*********	******	****	129.080	******

AMUR= 1.237 AMUW= 1.315 REAVG=827.411
PRAVG= 3.243 TWAVG=127.848 TBAVG=133.749
MEAN GRASHOF= .3C0377E+05 GRATZ = 13.937

CLIVERS CORRELATION---> NUSS= 6.782
THOMAS CORRELATION----> NUMT= 6.529
EXPERIMENTAL DATA-----> NUM = 7.174

Appendix B

Flow Model and Data

A computer program was written to solve for the flow distribution in the collector plumbing. As seen by Figure 21 there are twelve risers with twelve resistors. The headers have eleven resistors each. In the simplest form the flow and pressure drop are related by an equation of the following form:

$$\Delta P = RW^E \qquad \text{(B-1)}$$

Specifying the constants R and E the pressure drop can be found along the tube. Furthermore, as it is true for the electrical analog where the sum of the voltages equals zero in a loop, the sum of the pressure drops in a loop equals zero for fluid flow problems.

This was the fundamental principle of the flow model. Thus, specifying the constants and the total flowrate, the program adjusts the flows such that the pressure drop around each loop equals zero. The solution is then obtained. A listing of the program and sample output is included in this appendix.

The data used to generate Figure 18 and 20 was simply flowrate and temperature measurements. This data is listed in Tables B-I and B-II for the collector with and without turbulators, respectively.

The input data to the computer program is free format. Table B-III explains the input data. Following that table is a program listing and sample output.

Table B-I Temperature Measurements for Tubes With Turbulators (Clamped Fin)

	W (lbm/min) 2.0	4.125
T_{in}	137.46	135.4
T1	130.6	131.1
T2	132.04	132.4
T3	132.04	132.3
T4	131.5	132.2
T5	132.17	132.3
T6	131.5	131.5
T7	132.17	132.3
T8	132.04	132.4
T9	132.69	133.2
T10	131.78	132.5
T11	131.4	132.2
T12	127.8	130.1
T_{out}	130.4	131.8

AD-A091 085 AIR FORCE INST OF TECH WRIGHT-PATTERSON AFB OH SCHOO--ETC F/6 10/1
EXPERIMENTAL STUDY OF THE THERMAL PERFORMANCE PARAMETERS OF A L--ETC(U)
SEP 80 C D WOODRUM
UNCLASSIFIED AFIT/GAE/AA/80S-3 NL

END
DATE FILMED
12-80
DTIC

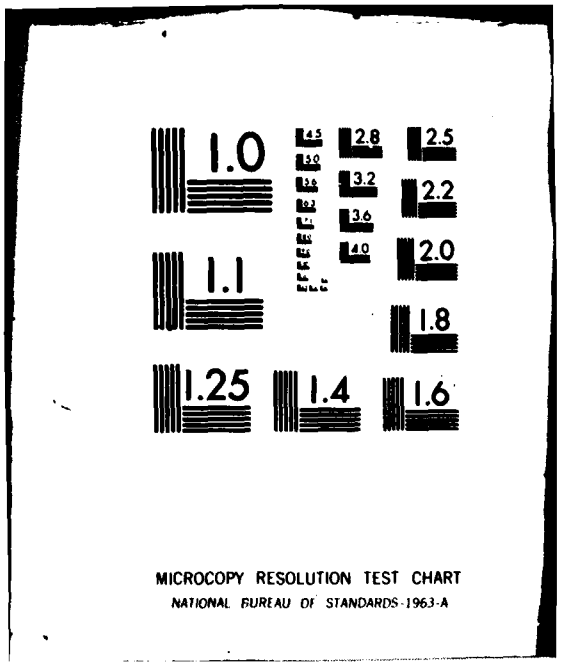
1.0
1.1
1.25
1.4
1.6
1.8
2.0
2.2
2.5
2.8
3.2
3.6
4.0
4.5
5.0
5.6
6.3
MICROCOPY RESOLUTION TEST CHART
NATIONAL BUREAU OF STANDARDS-1963-A

Table B-II Temperature Measurements for Tubes Without Turbulators (Clamped Fin)

	W (lbm/min)						
	.436	.983	1.42	1.96	2.63	3.04	
T_{in}	128.9	134.1	133.3	133	139	134.6	
T1	117.4	129.1	130.8	129.1	136.3	131.9	
T2	108.9	122.1	129.1	130.5	136.8	132.4	
T3	101.8	104	120.9	128.8	136.8	132.5	
T4	101.3	103.6	106.4	120.8	136.8	132.6	
T5	100.9	103.6	105.6	107.9	134.1	131.9	
T6	100.6	103.4	105.4	106.8	127.2	126.2	Temperature
T7	100.6	103.4	105.3	106.4	115.8	108.6	(degrees F)
T8	100.6	103.2	104.9	105.6	114.9	106.8	
T9	100.6	102.8	104.6	105.5	114.2	106	
T10	100.6	102.6	104.5	105.3	113.9	105.9	
T11	100.6	102.4	104.1	104.8	113.5	105.3	
T12	99.99	100.6	102.2	102.8	111.5	103	
T_{out}	112.92	124.6	126.6	127.5	134.2	130.5	
T	70	71	71	71	73	73	

Table B-II Continued

	W (lbm/min)						
	.641	1.7	1.94	1.93	2.67	4.44	6.71
T_{in}	123	135.9	130.9	127.6	138.2	134.7	131.9
T1	96.2	133.1	128.6	125.4	135.5	132	129.3
T2	117.1	132.4	128.8	125.6	135.8	132.3	129.7
T3	109.8	123.1	127.3	125.6	135.8	132.4	129.7
T4	98.7	105.4	119.1	120.8	134	132.5	130
T5	98.7	103.9	105.7	112.9	126	132.5	129.8
T6	98	103.9	103.9	105.3	110.4	132.6	130
T7	98	103.8	103.4	104.5	109.5	132.4	129.9
T8	97.9	103.6	103	104	108.9	132.2	129.9
T9	97.7	103.1	102.6	103.6	108.2	129.1	129.9
T10	97.6	102.8	102.4	103.4	108	104.2	129.9
T11	97.4	102.4	102	102.9	107.7	102.2	129.6
T12	95.5	100.6	100.4	101.2	104.4	100.4	128.3
T_{out}	112.72	129.7	126.1	122.1	132.4	131.4	129.2
T	72	69	69	68	64	72	75

Table B-III Flow Model Input Data

Card #	Data	Comment
1	1., 1500, 2	
2	4.	Flowrate (lbm/min)
3	.10375, .1017E-2, .1017E-2	
*		
*		
*	Constant, R, for the risers,	
*	upper and lower headers	
*	respectively in the equation	
*	$\Delta P = RW^E$	
*		
*		
14	.10375, .1017E-2, .1017E-2	
15	1.6036, 2., 2.	
*		
*		
*	Constant, E, for the risers,	
*	upper and lower headers	
*	respectively in the equation	
*	$\Delta P = RW^E$	
*		
*		
26	1.6036, 2., 2.	
27	0.	Exit pressure

```
      PROGRAM DANA (INPUT,OUTPUT)
      DIMENSION W(12),WX(12),WY(12)
      DIMENSION DELW(11),R(12),RX(12),RY(12),E(12),EX(12),EY(12)
      COMMON/FLOW/ W,WX,WY
      COMMON/RESIST/ R,RX,RY
      COMMON/EXPON/ E,EX,EY
      CALL DATA(WIN,PRI,MAX,IFRACT)
      CALL INITIAL(WIN,PRI)
      L=1
      K=1
10    CONTINUE
      CALL LOOP(L,DELW,BIG,IFRACT,MAX,IP,K)
      CALL NEWGUES(DELW,WIN)
      IF(K.EQ.IP) K=0
      IF(L.GT.MAX) GO TO 20
      L=L+1
      K=K+1
      GO TO 10
20    CALL PLOT
      STOP
      END

      SUBROUTINE DATA(WIN,PRI,MAX,IFRACT)
      DIMENSION R(12),RX(12),RY(12),E(12),EX(12),EY(12)
      COMMON/RESIST/ R,RX,RY
      COMMON/EXPON/ E,EX,EY
      READ *,PRI,MAX,IFRACT
      READ *,WIN
      DO 10 I=1,12
10    READ *,R(I),RX(I),RY(I)
      DO 25 I=1,12
25    READ *,E(I),EX(I),EY(I)
      IF(PRI.EQ.0.) GO TO 30
      PRINT 6
```

```
6       FORMAT(/)
        DO 2C I=1,12
        PRINT 5,I,R(I),I,RX(I),I,RY(I)
5       FORMAT(10X,*R(*,I2,*)=*,E12.6,5X,*RX(*,I2,*)=*,E12.6,
       $5X,*RY(*,I2,*)=*,E12.6)
20      CONTINUE
30      CONTINUE
        RETURN
        END


        SUBROUTINE INITIAL(WIN,PRI)
        DIMENSION W(12),WX(12),WY(12)
        COMMON/FLOW/ W,WX,WY
        DO 1C I=1,12
10      W(I)=WIN/12.
        X=WIN
        Y=0.
        DO 2C I=1,11
        WX(I)=X-W(I)
        X=X-1.
        WY(I)=Y+W(I)
20      Y=Y+1.
        IF(PRI.EQ.0) GO TO 30
        PRINT 6
6       FORMAT(//)
        DO 35 I=1,12
35      PRINT 5,I,W(I),I,WX(I),I,WY(I)
5       FORMAT(10X,*W*,I2,*=*,E15.6,5X,*WX*,I2,*=*,E15.6
       $,5X,*WY*,I2,*=*,E15.6)
30      CONTINUE
        RETURN
        END
```

```
      SUBROUTINE LOOP(L,DELW,BIG,IFRACT,MAX,IP,K)
      DIMENSION D(11),DD(11),R(12),RX(12),RY(12),DELW(11)
      DIMENSION W(12),WX(12),WY(12),E(12),EX(12),EY(12)
      DIMENSION RM(12)
      COMMON/FLOW/ W,WX,WY
      COMMON/RESIST/ R,RX,RY
      COMMON/EXPON/ E,EX,EY
      IP=MAX/IFRACT
      DO 10 I=1,11
      IF(W(I).LT.0) GO TO 50
      D(I)=R(I)*ABS(W(I))**E(I)
      GO TO 55
50    D(I)=-R(I)*ABS(W(I))**E(I)
55    IF(WY(I).LT.0) GO TO60
      D(I)=D(I)+RY(I)*ABS(WY(I))**EY(I)
      GO TO 65
60    D(I)=D(I)-RY(I)*ABS(WY(I))**EY(I)
65    IF(W(I+1).LT.0) GO TO 70
      D(I)=D(I)-R(I+1)*ABS(W(I+1))**E(I+1)
      GO TO 75
70    D(I)=D(I)+R(I+1)*ABS(W(I+1))**E(I+1)
75    IF(WX(I).LT.0) GO TO 80
      D(I)=D(I)-RX(I)*ABS(WX(I))**EX(I)
      GO TO 85
80    D(I)=D(I)+RX(I)*ABS(WX(I))**EX(I)
85    DD(I)=E(I)*R(I)*ABS(W(I))**(E(I)-1.)
      DD(I)=DD(I)+EY(I)*RY(I)*ABS(WY(I))**(EY(I)-1.)
      DD(I)=DD(I)+E(I+1)*R(I+1)*ABS(W(I+1))**(E(I+1)-1.)
      DD(I)=DD(I)+EX(I)*RX(I)*ABS(WX(I))**(EX(I)-1.)
      IF(DD(I).EQ.0.) PRINT 40,I,DD(I)
40    FORMAT(20X,*DD(*,I2,*)=*,E10.3,*  ERROR MODE 4 WILL RESULT*)
10    DELW(I)=D(I)/DD(I)
      IF(L.EQ.1.OR.K.EQ.IP) GO TO 99
      GO TO 37
99    PRINT 4,L
```

```
4     FORMAT(////,25X,*<<<<    ITERATION NUMBER*,I6,*    >>>>*)
      PRINT 63
63    FORMAT(/)
      DO 46 I=1,12
46    PRINT 45,I,W(I),I,WX(I),I,WY(I)
45    FORMAT(5X,*W*,I2,*=*,E15.7,5X,*WX*,I2,*=*,E15.7
     $,5X,*WY*,I2,*=*,E15.7)
      DO 20 I=1,11
      N=I+1
      PRINT 1,I
1     FORMAT(///10X,*LOOP*,I2,* RESULT SUMMARY*)
      PRINT 2,I,W(I),I,WY(I),N,W(I+1),I,WX(I)
2     FORMAT(/10X,*W*,I2,*=*,E15.7,5X,*WY*,I2,*=*,E15.7,
     $5X,*W*,I2,*=*,E15.7,5X,*WX*,I2,*=*,E15.7)
      PRINT 3,I,DELW(I),D(I),DD(I)
3     FORMAT(10X,*DELW(*,I2,*)=*,E15.7,5X,*LOOP DELP=*,E15.7,
     $5X,*LOOP DELPDOT=*,E15.7)
20    CONTINUE
      BIG=AMAX1(DELW(1),DELW(2))
      DO 30 I=1,9
30    BIG=AMAX1(BIG,DELW(I+2))
37    CONTINUE

      IF(L.EQ.1.OR.K.EQ.IP) PRINT 98,BIG
98    FORMAT(/20X,*MAXIMUM CORRECTIVE FLOW=*,E15.7)
      RETURN
      END
```

```
      SUBROUTINE NEWGUES(DELW,WIN)
      DIMENSION W(12),WX(12),WY(12),DELW(11)
      COMMON/FLOW/ W,WX,WY
      DO 50 I=1,12,11
      J=1
      IF(I.EQ.12) J=11
      IF(I.EQ.1)      W(I)=W(I)-DELW(J)
      IF(I.EQ.12)     W(I)=W(I)+DELW(J)
15    WY(J)=W(I)
50    CONTINUE
      DO 55 I=2,11
      DNET=DELW(I)-DELW(I-1)
      W(I)=W(I)-DNET
55    CONTINUE
      J=3
      DO 60 I=2,11
      WX(1)=WIN-W(1)
      WX(I)=WX(I-1)-W(I)
      WY(2)=WY(1)+W(2)
      WY(J)=WY(J-1)+W(J)
      J=J+1
      IF(I.EQ.11) WX(I)=W(12)
60    CONTINUE
      RETURN
      END

      SUBROUTINE PLOT
      COMMON/RESIST/ R,RX,RY
      COMMON/EXPON/ E,EX,EY
      COMMON/FLOW/ W,WX,WY
      DIMENSION R(12),RX(12),RY(12),E(12),EX(12),EY(12),W(12),WX(12),WY(
     $12)
      DIMENSION P(24),DELP(22)
```

```
      READ *,POUT
      P(24)=POUT
      P(12)=P(24)  +  P(12)*W(12)**E(12)
      DO 10 I=1,11
      DELP(I)=PY(12-I)*WY(12-I)**EY(12-I)
      DELP(I+11)=PX(12-I)*WX(12-I)**EX(12-I)
      P(24-I)=DELP(I)  +  P(25-I)
      P(12-I)=DELP(11+I)  +  P(13-I)
10    CONTINUE
      PRINT 15
15    FORMAT(1H1)
      DO 17 I=1,5
      PRINT 16
16    FORMAT(/)
17    CONTINUE
      PRINT 20
20    FORMAT(10X,*P13=*,6X,*P14=*,6X,*P15=*,6X,*P16=*,6X,*P17=*,6X,
     1*P18=*,6X,*P19=*,6X,*P20=*,6X,*P21=*,6X,*P22=*,6X,*P23=*,6X,
     1*P24=*)
      PRINT 25,(P(12+I),I=1,12)
25    FORMAT(10X,12F10.5)
      PRINT 30
30    FORMAT(10X,*----------------------------------------------------
     $----------------------------------------------------
     $*)
31    FORMAT( 1X,*----------------------------------------------------
     $----------------------------------------------------
     $*)
      DO 35 I=1,40
      PRINT 40
40    FORMAT(10X,*I*,9X,*I*,9X,*I*,9X,*I*,9X,*I*,9X,*I*,9X,*I*,9X,*I*,9X,*I*,9X
     $,*I*,9X,*I*,9X,*I*,9X,*I*)
35    CONTINUE
      PRINT 31
      PRINT 50
50    FORMAT(10X,*P 1=*,6X,*P 2=*,6X,*P 3=*,6X,*P 4=*,6X,*P 5=*,6X,*P 6=
```

```
     $*,6X,*P 7=*,6X,*P 8=*,6X,*P 9=*,6X,*P10=*,6X,*P11=*,6X,*P12=*)
      PRINT 60,(P(I),I=1,12)
60    FORMAT(10X,12F10.5)
      PRINT 65
65    FORMAT(///)
      DO 70 I=1,12
      PRINT 75,I,W(I),I,WX(I),I,WY(I)
75    FORMAT(10X,*W*,I2,*=*,E15.6,5X,*WX*,I2,*=*,E15.6
     $,5X,*WY*,I2,*=*,E15.6)
70    CONTINUE
      PRINT 65
      DO 80 I=1,12
      PRINT 85,I,R(I),I,RX(I),I,RY(I)
85    FORMAT(10X,*R(*,I2,*)=*,E12.6,5X,*RX(*,I2,*)=*,E12.6,
     $5X,*RY(*,I2,*)=*,E12.6)
80    CONTINUE
      PRINT 65
      DO 90 I=1,12
      PRINT 95,I,E(I),I,EX(I),I,EY(I)
95    FORMAT(10X,*E(*,I2,*)=*,E12.6,5X,*EX(*,I2,*)=*,E12.6,
     $5X,*EY(*,I2,*)=*,E12.6)
90    CONTINUE
      RETURN
      END
```

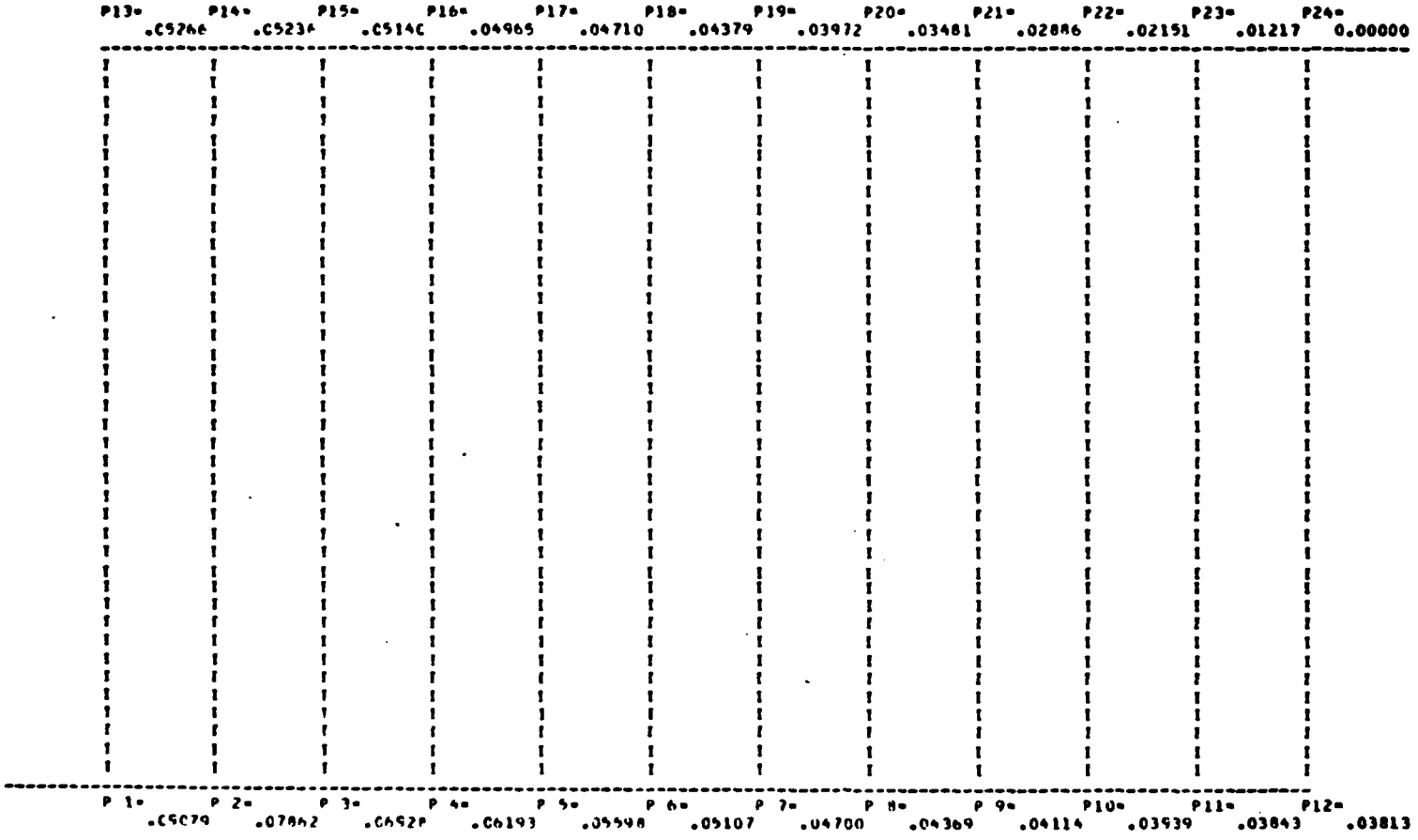
P13= .05766
P14= .05234
P15= .05140
P16= .04965
P17= .04710
P18= .04379
P19= .03972
P20= .03481
P21= .02886
P22= .02151
P23= .01217
P24= 0.00000
P 1= .05079
P 2= .07862
P 3= .06928
P 4= .06193
P 5= .05598
P 6= .05107
P 7= .04700
P 8= .04369
P 9= .04114
P10= .03939
P11= .03843
P12= .03813

W 1=	.541277E+00	WX 1=	.345872E+01	WY 1=	.541277E+00
W 2=	.430559E+00	WX 2=	.302816E+01	WY 2=	.971836E+00
W 3=	.340237E+00	WX 3=	.268793E+01	WY 3=	.131207E+01
W 4=	.270232E+00	WX 4=	.241769E+01	WY 4=	.158231E+01
W 5=	.221523E+00	WX 5=	.219617E+01	WY 5=	.180383E+01
W 6=	.196172E+00	WX 6=	.200000E+01	WY 6=	.200000E+01
W 7=	.196172E+00	WX 7=	.180383E+01	WY 7=	.219617E+01
W 8=	.221523E+00	WX 8=	.158231E+01	WY 8=	.241769E+01
W 9=	.270232E+00	WX 9=	.131207E+01	WY 9=	.268793E+01
W10=	.340237E+00	WX10=	.971836E+00	WY10=	.302816E+01
W11=	.430559E+00	WX11=	.541277E+00	WY11=	.345872E+01
W12=	.541277E+00	WX12=	0.	WY12=	.400000E+01

R(1)=	.103750E+00	RX(1)=	.101770E-02	RY(1)=	.101770E-02
R(2)=	.103750E+00	RX(2)=	.101770E-02	RY(2)=	.101770E-02
R(3)=	.103750E+00	RX(3)=	.101770E-02	RY(3)=	.101770E-02
R(4)=	.103750E+00	RX(4)=	.101770E-02	RY(4)=	.101770E-02
R(5)=	.103750E+00	RX(5)=	.101770E-02	RY(5)=	.101770E-02
R(6)=	.103750E+00	RX(6)=	.101770E-02	RY(6)=	.101770E-02
R(7)=	.103750E+00	RX(7)=	.101770E-02	RY(7)=	.101770E-02
R(8)=	.103750E+00	RX(8)=	.101770E-02	RY(8)=	.101770E-02
R(9)=	.103750E+00	RX(9)=	.101770E-02	RY(9)=	.101770E-02
R(10)=	.103750E+00	RX(10)=	.101770E-02	RY(10)=	.101770E-02
R(11)=	.103750E+00	RX(11)=	.101770E-02	RY(11)=	.101770E-02
R(12)=	.103750E+00	RX(12)=	.101770E-02	RY(12)=	.101770E-02

E(1)= .16306CE+01	EX(1)= .200000E+01	EY(1)= .20000CE+01
E(2)= .16306CE+01	EX(2)= .200000E+01	EY(2)= .20000CE+01
E(3)= .16306CE+01	EX(3)= .200000E+01	EY(3)= .20000CE+01
E(4)= .163060E+01	EX(4)= .200000E+01	EY(4)= .20000CE+01
E(5)= .16306CE+01	EX(5)= .200000E+01	EY(5)= .20000CE+01
E(6)= .16306CE+01	EX(6)= .200000E+01	EY(6)= .20000CE+01
E(7)= .16306CE+01	EX(7)= .200000E+01	EY(7)= .200000E+01
E(8)= .16306CE+01	EX(8)= .200000E+01	EY(8)= .20000CE+01
E(9)= .16306CE+01	EX(9)= .200000E+01	EY(9)= .20000CE+01
E(10)= .16306CE+01	EX(10)= .200000E+01	EY(10)= .20000CE+01
E(11)= .16306CE+01	EX(11)= .200000E+01	EY(11)= .20000CE+01
E(12)= .16306CE+01	EX(12)= .200000E+01	EY(12)= .20000CE+01

Appendix C

Bond Conductance Test

Kahn (Ref 6) evaluated the bond conductance of several materials using a simple indoor calorimetric test from which this test was derived. From Figure C-1 it is clear that the energy exchange can be written as follows which considers a fin-tube assembly receiving energy by radiation:

$$Q_u = C_b Y(t_w - t_f) \qquad \text{(C-1)}$$

where C_b = bond conductance (kb/s)
Y = length of fin-tube assembly
k = thermal conductivity.

This equation assumes negligible heat loss by radiation, conduction, and convection from the underside of the tube. Therefore, all that is necessary to measure the bond conductance is to measure the flowrate, temperature difference between the inlet and exit, and temperatures shown in Figure C-1.

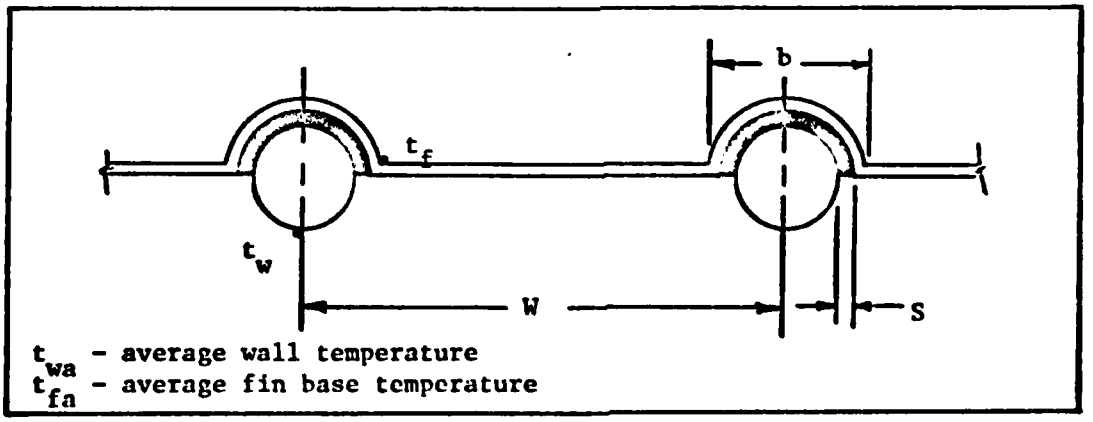

Figure C-1 Clamped Fin and Tube Arrangement

The test in this investigation was slightly different. Hot water was pumped through the system and no insulation was used to prevent heat loss from the tube to the atmosphere. Therefore, it was necessary to modify Eq (C-1) to account for this additional heat loss.

As discussed in Section III for the internal heat transfer coefficient test, high flowrates through the tubes make it possible to assume a linear wall temperature. This being the case the additional heat loss may be approximated by Eq (C-2):

$$Q_{loss} = \frac{h\pi DY}{2}(t_{wa} - t_{\infty}) + \sigma\frac{\pi DY}{2}(t_{wa} - t_{\infty}) \qquad (C-2)$$

where t_{∞} is the ambient temperature. The tube fits deep enough into the fin trough that free convection flow characteristics for heated plates facing downward probably more nearly typify conditions than flow around a cylinder, so the external heat transfer coefficient is given by (Ref 14:83):

$$Nu = .27(GrPr)^{.25} \qquad (C-3)$$

where the characteristic dimension has been taken as the fin width of four inches. Also, Eq (C-2) assumes blackbody radiation which tends to put a conservative estimate on the computed bond conductance.

Referring to the data in Table C-I, the average tube wall temperature, t_{wa}, is 119.53 F for the clamped fin of run number one. The ambient temperature, t_{∞}, is 52.01 F. With these values the calculation of the bond conductance is as follows:

$$Gr = \frac{\rho^2 g\beta}{\mu^2}(t_{wa} - t_\infty)X^3$$

$X = 4$ inches

$Pr = .72$

$Nu = 12.78$

$h = .57$ B/hr-ft^2-F

$$Q_{loss} = \frac{.57\pi(3)(4)}{(8)(12)(2)}(119.53 - 52.01) + \frac{.1714E\text{-}8(\pi)(3)(4)}{(8)(12)(2)}(579.53^4 - 512.01^4)$$

$$= 7.56 + 14.83$$

$$= 22.39 \text{ B/hr}$$

$$C_b = \frac{Q_u - Q_{loss}}{Y(t_{wa} - t_{fa})}$$

$$= \frac{WC_p(t_{fi} - t_{fo}) - Q_{loss}}{Y(t_{wa} - t_{fa})}$$

$$= \frac{.475(60)(129.98 - 121.59) - 22.39}{4(119.53 - 116.73)}$$

$$= 19.32 \text{ B/hr-ft-F}$$

The experimental set up was run twice with the woven fin as Table C-I shows. The purpose was to compare for the effectiveness of the thermal grease under that type configuration. The results show minimal improvement with the grease.

Table C-I Bond Conductance Test Results (Temperatures-deg F)

Run	Flowrate lbm/min C_b (B/hr-ft-F)	T1 T2 T3	T4 T5 T6	T7 T8 T9	T10 T11 T12	T13 T14
1	.475	129.98	123.01	120.56	119.01	115.53
	19.32	121.59	119.92	118.11	115.79	113.08
		52.01	100.44	99.15	99.15	
2	.958	131.66	127.53	124.82	124.30	121.59
	18.44	127.01	123.92	122.34	120.17	118.62
		50.26	101.99	100.7	102.31	
	a) Clamped Fin and Tube Results					
1	.2268	128.43	123.4	122.38	118.76	117.85
	1.06	120.69	103.4	99.15	108.95	90.38
		61.61	78.38	82.51	79.28	
2	.8362	134.88	131.78	131.01	128.43	127.4
	1.147	132.17	109.47	99.08	116.82	95.02
		62.12	78.77	85.73	82.38	
	b) Woven Fin and Tube Without Grease					
1	.3826	125.34	120.3	119.66	117.08	115.53
	1.77	119.4	105.73	97.21	107.27	96.18
		61.99	78.77	83.28	82.38	
2	.862	131.27	128.18	127.4	124.82	123.27
	1.37	128.82	111.4	101.34	113.6	100.69
		63.29	80.57	86.12	84.83	
	c) Woven Fin and Tube With Grease					

Appendix D

Overall Loss Coefficient

The overall loss coefficient may be calculated from classical techniques although the procedure is rather lengthy. This section summarizes the ways heat is lost and presents the methodology for computing the loss coefficient. At the end of this section a graph has been presented showing the overall loss coefficient as a function of plate temperature. Back, edges, and top losses all make up the overall loss coefficient and strictly speaking each is a function of the plate temperature, but the dependency is very weak. Therefore, Figure D-1 assumes the overall loss coefficient is a function of temperature only through the top loss coefficient.

Back Losses

Heat losses start at the bottom of the plate, travel through a .5 inch airspace, through 3.5 inches of insulation, .25 inches of plywood, and then to the atmosphere. Thus, convection and radiation is considered between the bottom of the absorber plate and the top of the fiberglass insulation. Conduction occurs through the insulation and plywood. Finally, convection and radiation to the atmosphere occurs.

Assuming the following quantities it can be shown that the back loss coefficient calculations result in a value of .0864 B/hr-ft^2-F:

$k_{insulation}$ = .028 B/hr-ft-F

$k_{plywood}$ = .07 B/hr-ft-F

ϵ_{plate} = .89

$\epsilon_{insulation}$ = .8

t_p = 135 F (plate temperature)

$\Delta t_{p\text{-insulation}}$ = 25 F

h_o = 2 B/hr-ft^2-F

External radiation is neglected.

Edge Loss

For this calculation it was assumed that heat is lost out the edge through a three inch vertical pine wood surface one inch thick and one inch of insulation. The edge area was computed as 4.22 square feet, and the collector area was computed as 17.758 square feet. Using a conductivity of .079 B/hr-ft-F for pine wood, the edge loss comes to .058 B/hr-ft^2-F.

Top Loss Coefficient

A computer program was written to model Klien's equation (Ref 2:133) for the top loss coefficient as a function of plate temperature. The tilt angle was taken as 50 degrees, the number of covers was two, the plate and glass emissivities were .89 and .88 respectively, and the wind velocity was taken as zero. A value of 2.0 B/hr-ft^2-F was used for the external heat transfer coefficient. The values of the back and edge overall loss coefficients were simply added to the resulting top loss coefficient at every plate temperature to obtain the collector overall loss coefficient. The result is given for two ambient temperatures in Figure D-1.

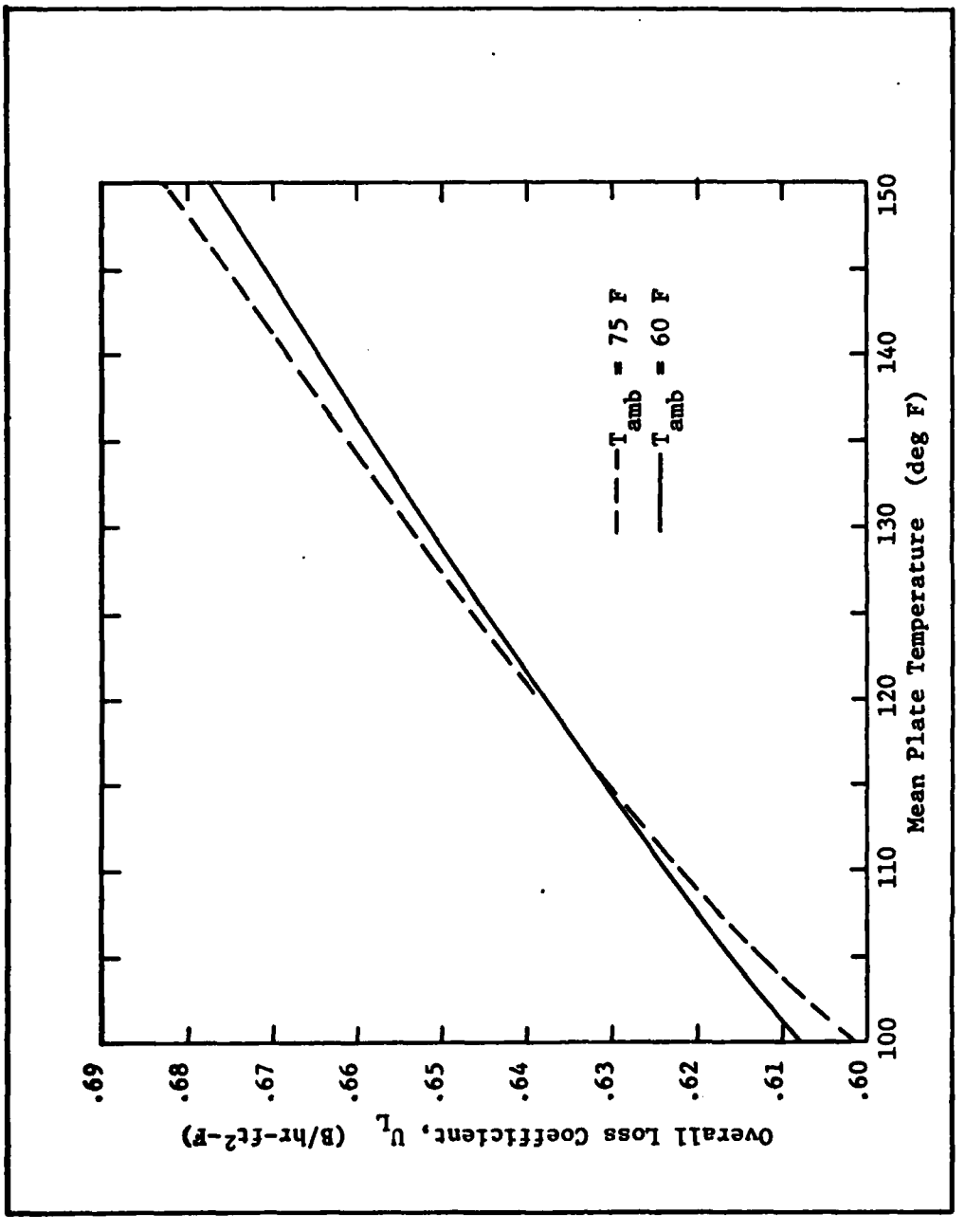

Figure D-1 Collector Overall Loss Coefficient as a Function of Mean Plate Temperature

Appendix E

$U_L F_R$ Product

Two methods were used to compute the overall loss coefficient, fin efficiency, collector efficiency factor, and the heat removal factor from measured data. The method is outlined and sample calculations are provided here.

Method 1

Taking a flowrate of .641 lbm/min from Table II, the measured $U_L F_R$ product was .437 B/hr-ft^2-F. From Table B-II the inlet and exit temperatures are 123.0 F and 112.72 F respectively. The average of these gives a thermal conductivity of water of .37 B/hr-ft-F. Using a mean Nusselt number of 7.21 the resulting heat transfer coefficient becomes 102.4 B/hr-ft^2-F. (This mean Nusselt number was used for all flowrates without turbulators.) Using a value of 17.758 ft^2 of collector area and a constant specific heat of water of 1 B/lbm-F, Eq (21) results in

$$U_L F' = .4881$$

Substituting the expression of F' from Eq (4) into the above and using the following quantities, an equation with the overall loss coefficient as the only unknown results:

δ = .035 inches
k = 26 B/hr-ft-F
D = 7/16 inch
L = 4 inches
C_b = 18.88 B/hr-ft-F

$$\frac{1}{\frac{4}{U_L\left[.4375 + 3.562\,\frac{\tanh .539(U_L)^{.5}}{.539(U_L)^{.5}}\right]} + .0574} - .4881 = 0 \qquad \text{(E-1)}$$

The iterative solution to Eq (E-1) is $U_L = .525$. Subsequently, F = .952, F' = .931, and $F_R = .833$.

Method 2

The average plate temperature from Table B-II is 100 F. Using Figure D-1, the overall loss coefficient is computed to be .608 B/hr-ft^2-F. The enthalpy change divided by the collector area gives

$$\frac{Q_u}{A_c} = \frac{.641(1)}{17.758}(60)(123.02 - 112.72) = 22.307$$

Using Eq (10) and (11) the mean plate temperature is given by

$$t_{pm} = 121.74 - \frac{22.307}{U_L F_R}\left[1 - \frac{F_R}{F'}\right]$$

Assuming $U_L = .608$ B/hr-ft^2-F the following quantities result:

$$F = .945$$
$$F' = .922$$
$$F_R = .813$$

Recomputing the mean plate with these quantities gives 116.4 F. Repeating the process a second time is quite sufficient. The ultimate solution becomes

$$U_L = .632 \text{ B/hr-ft}^2\text{-F}$$
$$F = .943$$

$$F' = .918$$

$$F_R = .805$$

$$U_L F_R = .509 \text{ B/hr-ft}^2\text{-F}$$

$$t_{pm} = 116 \text{ F}$$

Data

The required data for the clamped fin (Table II) is given in Table B-I and B-II. The woven fin data is summarized in Table E-I.

Table E-I Flowrate and Temperature Measurements for Tubes With and Without Turbulators for the Woven Fin

Without Turbulators			
Flowrate (lbm/min)	T_{in}	T_{out}	T_{amb}
1.687	141.3	135.4	73
2.75	141.7	137.7	72
4.28	139.8	136.6	72
7.45	139.8	137.2	72
9.0	138	135.9	72
With Turbulators			
Flowrate (lbm/min)	T_{in}	T_{out}	T_{amb}
1.5	134.4	124.2	68
2.56	135.4	129.7	68
5.96	137.9	133.6	68

Vita

Charles Dana Woodrum, a native of Bloomfield, Kentucky, was born on 21 January 1949. He was the grandson of a Kentucky dairy farmer, and until entering college at Union University, Jackson, Tennessee, he too was firmly established in that trade. After two years at Union University, he transferred to the University of Kentucky where he subsequently received his Bachelor of Science in Mechanical Engineering in December 1971 and also received a commission in the United States Marine Corps.

After serving for three years he returned to the University of Kentucky and began working towards a master's degree in Mechanical Engineering. Upon completing one semester of graduate study, he was employed at Wright Patterson AFB as a civilian and began his present studies at the Air Force Institute of Technology in March 1976.

Permanent Address: 4000 Tonawanda Trail
Dayton, Ohio 45430

SECURITY CLASSIFICATION OF THIS PAGE (When Data Entered)

REPORT DOCUMENTATION PAGE

READ INSTRUCTIONS BEFORE COMPLETING FORM

1. REPORT NUMBER: AFIT/GAE/AA/80S-3
2. GOVT ACCESSION NO: AD-A091085
3. RECIPIENT'S CATALOG NUMBER:

4. TITLE (and Subtitle): EXPERIMENTAL STUDY OF THE THERMAL PERFORMANCE PARAMETERS OF A LIQUID-HEATING FLAT PLATE SOLAR COLLECTOR

5. TYPE OF REPORT & PERIOD COVERED: M.S. Thesis

6. PERFORMING ORG. REPORT NUMBER:

7. AUTHOR(s): Charles Dana Woodrum

8. CONTRACT OR GRANT NUMBER(s):

9. PERFORMING ORGANIZATION NAME AND ADDRESS: Air Force Institute of Technology (AFIT/EN) Wright-Patterson AFB OH 45433

10. PROGRAM ELEMENT, PROJECT, TASK AREA & WORK UNIT NUMBERS:

11. CONTROLLING OFFICE NAME AND ADDRESS:

12. REPORT DATE: September 1980

13. NUMBER OF PAGES: 108

14. MONITORING AGENCY NAME & ADDRESS (if different from Controlling Office):

15. SECURITY CLASS. (of this report): UNCLASSIFIED

15a. DECLASSIFICATION DOWNGRADING SCHEDULE:

16. DISTRIBUTION STATEMENT (of this Report)

Approved for public release; distribution unlimited

17. DISTRIBUTION STATEMENT (of the abstract entered in Block 20, if different from Report)

18. SUPPLEMENTARY NOTES

19. KEY WORDS (Continue on reverse side if necessary and identify by block number)

Solar Energy
Thermal Performance
Flat Plate Solar Collector

20. ABSTRACT (Continue on reverse side if necessary and identify by block number)

Five tests were conducted on a 4X4 foot liquid-heating flat plate solar collector for:

(1) Internal heat transfer coefficient-with and without turbulators
(2) Flow distribution
(3) Bond conductance-clamped and woven fins
(4) Long wavelength transmittance of Kalwall
(5) Overall loss coefficient-heat removal factor product.

DD FORM 1 JAN 73 1473 EDITION OF 1 NOV 65 IS OBSOLETE

SECURITY CLASSIFICATION OF THIS PAGE (When Data Entered)

A

Mean values of the internal heat transfer coefficients ranged between 98-114 B/hr-ft^2-F for tubes without turbulators. Values as high as 522 B/hr-ft^2-F were obtained with turbulators. The flow distribution was determined to be satisfactory if turbulators were left in the risers. Non-uniform flow occurred without them as evidenced by temperature differences as high as 30 F between the collector inlet and tube wall temperatures (measured midway between the headers). Bond conductance values ranged from 18.88 B/hr-ft-F to 1.57 B/hr-ft-F for the clamped and woven fins, respectively. The transmittance for .025 inch Kalwall at long wavelengths was determined to be on the order of five percent. The overall loss coefficient was not successfully measured, but based on a previously determined value of it, the heat removal factor as a function of flowrate was compared for all configurations.